Solar and Interplanetary Sources of Major Geomagnetic Storms ($Dst \leq -100$ nT) During 1996 – 2005

J. Zhang,[1] I. G. Richardson,[2,3] D. F. Webb,[4] N. Gopalswamy,[2] E. Huttunen,[5] J. Kasper,[6] N. Nitta,[7] W. Poomvises,[1] B. J. Thompson,[2] C.-C. Wu,[2,8] S. Yashiro,[2,9] and A. Zhukov,[10,11]

Abstract.
We present the results of an investigation of the sequence of events from the Sun to the Earth that ultimately led to the 88 major geomagnetic storms (defined by minimum $Dst \leq -100$ nT) that occurred during 1996 - 2005. The results are achieved through cooperative efforts that originated at the Living with a Star (LWS) Coordinated Data-Analysis Workshop (CDAW) held at George Mason University in March 2005. Based on careful examination of the complete array of solar and in-situ solar wind observations, we have identified and characterized, for each major geomagnetic storm, the overall solar-interplanetary (solar-IP) source type, the time, velocity and angular width of the source coronal mass ejection (CME), the type and heliographic location of the solar source region, the structure of the transient solar wind flow with the storm-driving component specified, the arrival time of shock/disturbance, and the start and ending times of the corresponding IP CME (ICME). The storm-driving component, which possesses a prolonged and enhanced southward magnetic field (B_s), may be an ICME, the sheath of shocked plasma (SH) upstream of an ICME, a corotating interaction region (CIR), or a combination of these structures. We classify the Solar-IP sources into three broad types: (1) S-type, in which the storm is associated with a single ICME and a single CME at the Sun; (2) M-type, in which the storm is associated with a complex solar wind flow produced by multiple interacting ICMEs arising from multiple halo CMEs launched from the Sun in a short period; (3) C-type, in which the storm is associated with a CIR formed at the leading edge of a high speed stream originating from a solar coronal hole (CH). For the 88 major storms, the S-type, M-type and C-type events number 53 (60%), 24 (27%) and 11 (13%), respectively. For the 85 events for which the surface source regions could be investigated, 54 (63%) of the storms originated in solar active regions, 10 (12%) in quiet Sun regions associated with quiescent filaments or filament channels, and 11 (13%) were associated with coronal holes. Remarkably, 10 (12%) CME-driven events showed no sign of eruptive features on the surface (e.g., no flare, no coronal dimming, and no loop arcade, etc), even though all the available solar observation in a suitable time period were carefully examined. Thus, while it is generally true that a major geomagnetic storm is more likely to be driven by a front-side fast halo CME associated with a major flare, our study indicates a broad distribution of source properties. The implications of the results for space weather forecasting are briefly discussed.

1. Introduction

A NASA Living With a Star (LWS) Coordinated Data Analysis Workshop (CDAW) was held at George Mason University, Fairfax, VA, in March 2005. The workshop focused on the major geomagnetic storms of solar cycle 23, specifically the 88 events from 1996 (corresponding to the start of observations from the SOHO spacecraft) to the end of 2005 having minimum Dst (disturbance storm time index) $\leq$ -100 nT. Four working groups were established to address (1) the solar and interplanetary (IP) sources of these storms, (2) storm mechanisms, (3) the associated ionospheric storms, and (4) storm predictions. Here, we summarize the efforts of Working Group 1 to identify the sequence of Sun-to-Earth activities for all 88 storms. The aim was to produce as comprehensive a list of solar-IP sources as possible by combining a wide variety of data sets and exploiting the different areas of expertize of the group members. The purpose of this paper is to describe the identification methods and present the identification results, which we hope will serve as a basis for further in-depth studies of these important Sun-Earth connection events.

It is now well established that a geomagnetic storm is the consequence of a chain of causative events originating from the Sun's corona and ultimately evolving into a geo-effective solar wind flow in near-Earth space [e.g., *Brueckner et al.*, 1998; *Webb et al.*, 2001; *Berdichevsky et al.*, 2002; *Zhang et al.*, 2003; *Gopalswamy et al.*, 2005]. Such geo-effective solar wind flows fall into two broad types, depending on their origins. One type is associated with an IP coronal mass ejection (ICME, also known as ejecta), the interplanetary counterparts of CMEs at the Sun, and includes the disturbed shock sheath (SH) region upstream of the ICME (which may have a shock at the leading edge) and the ICME itself. The second type is associated with fast solar wind emanating from solar coronal holes, in particular with the corotating interaction regions (CIRs) that form at the leading edges of such streams as they interact with the preceding slower ambient solar wind. Previous studies have found that major/intense geomagnetic storms (e.g., $Dst \leq$ -100 nT, or $Kp \geq 7-$) are mainly caused by ICMEs, while moderate and minor storms can be caused by both ICMEs and CIRs [*Gosling et al.*, 1991; *Tsurutani and Gonzalez*, 1997; *Richardson et al.*, 2002]. Nevertheless, recent studies showed that some major storms may be driven by CIRs [*Zhang et al.*, 2003; *Richardson et al.*, 2006], although their Dst values were not too far below -100 nT. Regardless of the solar origin, the geo-effective solar wind is usually a period of with prolonged and enhanced southward-directed magnetic field (B_s) that allows efficient solar wind energy transport into the Earth's magnetosphere [e.g., *Dungey*, 1961; *Gonzalez et al.*, 1994]. This enhanced B_s field could be embedded within any part (front or rear) of ICMEs, SHs and CIRs [e.g., *Crooker et al.*, 1992; *Wu and Lepping*, 2002; *Huttunen and Koskinen*, 2004; *Richardson et al.*, 2006].

Routine associations between ICMEs observed in geospace and CMEs observed at the Sun became possible after the launch of the SOHO spacecraft. Because of unfavorable launching directions and limited angular spans, the majority of CMEs do not intercept the Earth. However, a front-side halo CME, which appears as an expanding circular feature surrounding the coronagraph occulting disk and thus likely has component moving toward the Earth along the Sun-Earth line, is likely to produce an ICME at the Earth [*Howard et al.*, 1982]. Comprehensive association work, based on a large number of CMEs and ICMEs continuously observed over years, have been carried out [e.g., *Lindsay et al.*, 1999; *Gopalswamy et al.*, 2000; *Cane and Richardson*, 2003; *Schwenn et al.*, 2005]. In general, based on existing solar and solar wind observations, one is able to make unique CME-ICME association for about half of all ICME events. However, reliable one-to-one associations for other ICMEs becomes more difficult, mainly because multiple activity at the Sun results in complex interplanetary flows or compound streams [*Gopalswamy et al.*, 2001; *Burlaga et al.*, 2002; *Zhang et al.*, 2003] or provides several plausible candidate associations. Further, a number of ICMEs, including those causing major geomagnetic storms, were found not to be associated with any identifiable front-side halo CMEs [*Zhang et al.*, 2003; *Schwenn et al.*, 2005]

In this paper, our focus is to identify the solar and IP sources that lead to major geomagnetic storms. Our comprehensive search for the sequence of events includes the solar surface sources, flare activity, CMEs, ICMEs and CIRs. Various tracking methods are used to address not only the obvious one-to-one events, but also to provide the possible sequences for all complex events and problem events as well. While the evolution of an event is from the Sun to the Earth, it is practical to work backward from the Earth to the Sun for reliable identifications. The organization of the paper is as follows: Section 2 discusses the selection of the major geomagnetic storms. In section 3, we describe the methods used to identify the IP and solar sources of these geomagnetic storms. In section 4, we list the properties of the identified solar and IP sources and discuss the statistical results. Section 5 summarize the results of this paper.

[1]Department of Computational and Data Sciences, George Mason University, USA.

[2]NASA Goddard Space Flight Center, Greenbelt, Maryland, USA.

[3]Department of Astronomy, University of Maryland, College Park, Maryland, USA

[4]Inst. for Scientific Research, Boston College

[5]University of California at Berkeley, USA.

[6]MIT Center for Space Research

[7]LMSAL, USA.

[8]CSPAR, University of Alabama in Huntsville, USA.

[9]Catholic University of America, USA

[10]Royal Observatory of Belgium

[11]Skobeltsyn Institute of Nuclear Physics, Moscow State University, Russia

0148-0227/07/$9.00

2. Selection of Major Geomagnetic Storms

The workshop focused on the major geomagnetic storms that occurred between January 1996 and December 2005. This 10-year period extends from the start to most of the descending phase of solar cycle 23, which had two sunspot maxima in 2000 and 2001. The *Dst* index is a measure of the strength of the ring current and widely used for measuring the intensity of geomagnetic storms. We defined a major geomagnetic storm as a minimum in hourly *Dst* index falling below -100 nT. A similar threshold for major/intense storms has been used by other authors [e.g., *Tsurutani et al.*, 1997]. Other indices may be used, such as the *Kp* index [e.g., *Gosling et al.*, 1991; *Richardson et al.*, 2002]. Further, if a period of high activity showed multiple $Dst \leq -100$ nT minima, we arbitrarily assigned these to a single storm event if the minima were separated by less than 24 hours, rather than define each minimum as a separate storm (except the two storms that occurred at 12 UT, August 6 and 06 UT, August 7, 1998, which corresponded to two well separated ICMEs). As will be noted later, both single and multiple solar CMEs were found to be responsible for minima within a "single" storm event.

We identified 88 major geomagnetic storms in total from January 1996 to December 2005, using the selection criteria described above. The events through 2003 are based on the final *Dst* index, whereas those in 2004 and 2005 are based on the provisional *Dst* index, so it is possible that they may be adjusted slightly based on the final index. (*Dst* data are obtained at http://swdcdb.kugi.kyoto-u.ac.jp/dstdir/index.html). The 88 storms are listed in Table 1, where the first three columns indicate the event reference number, the storm peak time and the minimum *Dst* value, respectively. The other columns, which will be explained later, describe the parameters for the solar and IP sources.

Figure 1 shows the distributions of the storm strength (top panel), yearly occurrence rate (middle panel) and occurrence rate as a function of calendar month (bottom panel). A majority of these events (60 out of 88; 68%) have minimum *Dst* between -100 nT and -150 nT. A further 10 events (11%) have minimum *Dst* between -150 nT and -200 nT. There are 18 "severe" storms (21%) with minimum $Dst \leq -200$ nT. The largest geomagnetic storm ($Dst = -422$ nT) occurred on November 20, 2003 [*Gopalswamy et al.*, 2005]. The yearly major storm occurrence rate was highest (~ 13 events per year) during 2000 – 2002 around the time of maximum sunspot number (SSN). The occurrence rate was lowest in 1996 at solar minimum. The bottom panel of Figure 1 shows that the occurrence of major storms in general follows the well known semiannual variation of geomagnetic activity [e.g., *Russell and McPherron*, 1973; *Cliver et al.*, 2002], that is, higher activity during the equinoctial months and lower activity around the solstitial months. The number of major storms peaks in April–May and in October–November, and is lowest in June and in December (when no storms occurred). Interestingly, the number of major storms around the fall equinox is almost twice that at the spring equinox, and there are 55 events during the second half of year compared with only 33 during the first half.

3. Methods of Identifying Solar-IP Sources of Major Storms

3.1. Identifying and Characterizing the IP Sources

The primary physical mechanism for energy transfer from the solar wind to the magnetosphere is magnetic reconnection between the IMF and the Earth's magnetic field. The efficiency of this process mainly depends on the strength of the southward IMF, or more accurately, the dawn-dusk ($-y$) component of the electric field ($\mathbf{E} = -\mathbf{V} \times \mathbf{B}$) [e.g., *Dungey*, 1961; *Perreault and Akasofu*, 1978; *Tsurutani and Gonzalez*, 1997]. One formulation for the Dst index [*O'Brien and McPherron*, 2000] relates the (pressure-corrected) Dst^* index to the solar wind driver given by VB_s, where VB_s is the rectified value of VB_z that is positive when B_z is southward and zero when B_z is northward. The equations are:

$$\frac{d}{dt}Dst^* = Q(VB_s) - \frac{Dst^*}{\tau(VB_s)}, \tag{1}$$

$$Q(VB_s) = \begin{cases} \alpha(VB_s - E_c) & VB_s > E_c, \\ 0 & VB_s \leq E_c, \end{cases} \tag{2}$$

$$\tau(VB_s) = \tau_\infty \exp(\frac{V_o}{V_q + VB_s}). \tag{3}$$

The rate of change of Dst^* is assumed to be proportional to VB_s (Q representing injection into the ring current) less a loss term represented by the recovery time τ that depends on the strength of the ring current and is assumed to be proportional to Dst^*.

Since storms are driven by the solar wind magnetic fields and plasma impinging on the Earth, we used in-situ solar wind plasma and magnetic field observations from the Advanced Composition Explorer (ACE) and WIND spacecraft to identify the IP sources of the geomagnetic storms in this study. For ACE data, covering events during early 1998 – 2005, 64-s resolution data were examined. We also examined solar wind ion composition data from the ACE/SWICS instrument. ACE is in orbit at the upstream L1 point, so there is typically a $\sim 20 - 60$ minute delay for solar wind structures to transit from ACE to the Earth. For WIND data, 92-s resolution data were used. During the period of this study, WIND spacecraft executed a complicated trajectory in the near-Earth solar wind with a variable solar wind transit time delay of typically less than 1 hour. Because of the near-complete observations provided by two spacecraft together, we were able to deduce the IP sources for all 88 major geomagnetic storms studied.

Based on their plasma and magnetic signatures, we identified various types of structures in the near-Eath solar wind in association with the geomagnetic storms. These include ICME-driven shocks, SHs, ICMEs including magnetic clouds (MCs)(a sub-set of ICMEs in which the magnetic field is enhanced and rotates through a large angle [*Klein and Burlaga*, 1982]), and CIRs. To assist in these identification, we referred to the several existing catalogs. For shocks, we used the WIND shock list compiled by J. Kasper (MIT) (*http://space.mit.edu/home/jck/shockdb/shockdb.html*), and the ACE shock list compiled by C. W. Smith (UNH) (*http://www−ssg.sr.unh.edu/mag/ace/ACElists/obs$_l$ist.html*). For ICMEs, we referred to an updated version of the "comprehensive" ICME list compiled by *Cane and Richardson* [2003]. In addition, we used lists of MCs and "cloud-like" ICMEs compiled by R. P. Lepping and C.-C. Wu (*http://lepmfi.gsfc.nasa.gov/mfi/MCL1.html*) [*Lepping et al.*, 2005] and the magnetic cloud list of *Huttunen et al.* [2005]. Considering plasma composition and charge states, we used the list of high Fe-charge state intervals that are frequently associated with ICMEs, compiled by *Lepri et al.* [2001], supplemented by information on compositional and charge state anomalies, also typically associated with ICMEs, based on the study of *Richardson and Cane* [2004].

The storm of July 27, 2004 (Event 75 in Table 1) serves to illustrate the method of source identification, as shown in Figure 2. The top panel shows the Dst index, indicating that this storm had a minimum value of $Dst = -197$ nT at 14 UT. The following five panels show time profiles of the IMF strength and north-south (z) component, velocity, proton density, proton temperature and calculated plasma β, respectively. The three solar images at the bottom will be explained later. The IP driver of the main phase of the storm was evidently the extended interval of southward magnetic field reaching values of ~ 20 nT that started at ~ 05 UT on July 27, and lasted for about 10 hours. There was also a separate interval of southward field from ~ 22 UT on July 26 to ~ 02 UT on July 27 that depressed Dst just below -100 nT at ~ 3 UT. Dst then recovered in response to a northward turning of the IMF; note the ~ 2 hour delay in the Dst response due to the solar wind transit time from ACE and magnetospheric effects.

Examining the broader context of the solar wind driver, we identified the passage of a fast forward IP shock at 22:27 UT (at ACE; 22:25 UT at WIND) on July 26 (indicated by the vertical red line in Figure 2), characterized by abrupt jumps in the solar wind magnetic field, speed, density and temperature. The shock was followed by a "sheath" of shocked IP plasma characterized by enhanced, fluctuating field strength, speed, density and temperature, extending for about 4-hours.

The interval between the two blue vertical lines is the probable time of passage of the ICME that was driving this shock. The signatures of ICMEs have been discussed extensively [e.g., *Neugebauer and Goldstein*, 1997; *Wimmer-Schweingruber et al.*, 2006; *Zurbuchen and Richardson*, 2006]. Here, we note the abnormally low proton temperature, depressed below the expected temperature for normal solar wind [*Richardson and Cane*, 1995] overlaid in red, together with the enhanced magnetic field, smooth rotation in field direction (evident in B_z), and low plasma β that is characteristic of a MC. Other signatures (not shown here) include enhanced oxygen charge states observed by ACE/SWICS and bidirectional suptrathermal electron flows observed by the ACE solar wind plasma instrument. Thus, the extended region of southward field driving the main phase of this storm was associated with the passage of a MC. The short period of southward field producing the initial phase of the storm was associated with the sheath of shocked plasma ahead of the MC. Compressed magnetic fields in sheath regions may be draped over around the approaching ICME [e.g. *Gosling and McComas*, 1987]. This may lead to strong out of the ecliptic fields, perhaps accounting for the initial phase of this storm. Two notable features of this event are the high solar wind speeds, reaching ~ 1000 km/s, in the SH and MC, and the overall low solar wind densities compared to average values.

Considering CIRs, regions of compressed plasma formed by the interaction of high-speed streams from coronal holes with the preceding slower solar wind, these can be recognized by their characteristic variations in plasma parameters, including enhancements in the magnetic field strength, plasma density, temperature, and flow deflections lying at the leading edges of corotating high-speed streams [e.g., *Forsyth and Marsch*, 1999] and references therein. Examples of major storms in our study driven by CIRs have been illustrated by *Richardson et al.* [2006], so a sample event will not be discussed in the present paper. For a recent review of CIRs and associated geomagnetic activity, see the papers in *Tsurutani et al.* [2006].

3.2. Identifying Solar Sources

To identify the solar sources of the IP structures such as ICMEs that drive the major storms studied, we predominantly used observations from instruments on the SOHO spacecraft. CMEs near the Sun are observed by the LASCO

C2 and C3 coronagraphs, which have fields of view of 2 – 6 R_s and 4 – 30 R_s, respectively [*Brueckner et al.*, 1995]. There were LASCO observations for 80 of the 88 major geomagnetic storms studied. The 8 events with LASCO data gaps occurred mostly in 1998 and 1999 when SOHO lost control for many months. To identify the surface features of CMEs in the source region, observations from SOHO's Extreme-Ultraviolet Imaging Telescope (EIT) [*Delaboudiniere et al.*, 1995], which images the Sun's corona over the full disk and up to 1.5 R_s, were used, in particular those in the 195 Å passband which is dominated by Fe XII emission and sensitive to a plasma temperature of about 1.5 MK. In addition to referring to the LASCO CME catalog generated by NASA and The Catholic University of America in cooperation with the Naval Research Laboratory [*Yashiro et al.*, 2004] (*http://cdaw.gsfc.nasa.gov/CME_list/*), we also carefully examined all the LASCO and EIT images in a suitable period prior to each storm to search for any eruption features that might not have been included in the catalog, and to confirm the nature of the cataloged events. The Michelson Doppler Imager (MDI [*Scherrer et al.*, 1995] provided photospheric magnetograms.

In addition to SOHO observations, we used "traditional" synoptic data, such as daily NOAA solar event reports, which include data on soft X-ray flares, filament eruptions and active regions (*http://www.sec.noaa.gov/ftpdir/indices/*). These data complement and reinforce the SOHO LASCO/EIT observations. We have also used X-ray coronal images made by the Yohkoh Soft X-ray Telescope (SXT) [*Tsuneta et al.*, 1991] while it was available (Yohkoh was permanently lost in December 2001) to search for possible eruption signatures. X-ray imaging observations made by the Soft X-ray Imager (SXI) on the GOES satellites [*Hill et al.*, 2005] have also been used when available. For events from February 2003 onward, observations from the Solar Mass Ejection Imager (SMEI) [*Jackson et al.*, 2004; *Webb et al.*, 2006] were used to help track CMEs to larger distances from the Sun than is possible with LASCO.

The method of identifying the corresponding solar source of an existing ICME is straightforward, albeit ambiguous in many cases, that is to find a front-side halo (partial or full) CME at a reasonably earlier time, which depends on the transit time of the CME from the Sun to the Earth [e.g. *Webb et al.*, 2000; *Zhang et al.*, 2003]. The justification of this method is that there must be a cause-and-effect relationship between solar and IP events, even though current observations only cover the near-Sun space, through remote-sensing, and the near-Earth space through in-situ sampling. However, the lack of imaging observations in the vast region between the Sun and the Earth through which CMEs can travel for days without direct tracking, contribute to the ambiguity of any such associations.

Among the many CMEs observed at the Sun, halo CMEs, seen as an expanding circular bright feature fully surrounding the coronagraph occulting disk (augular width 360°), are believed most likely to hit the Earth [e.g., *Howard et al.*, 1982]. The large angular width observed is attributed both to the projection effect and a large intrinsic width, indicating the CME axis is likely directed along the Sun-Earth line, either toward the Earth if originating from the front-side of the Sun, or away from the Earth if originating from the back-side of the Sun. In addition to "full" halo CMEs, we also consider "partial halo" CMEs (apparent angular width $\geq 120°$) in the solar source identification. To verify the surface source region of a CME, we mainly use EIT observations, which often manifest the CME origin with several eruptive features, including large scale coronal dimming [e.g., *Thompson et al.*, 1998] and post-eruption loop arcade (the counterpart of the more familiar post-flare loop arcade in H_α). These eruptive features are often associated with localized coronal brightenings (the counterparts of flares in EUV wavelength).

Considering the complexity in associating CMEs with ICMEs, we exploited an iterative process with multiple steps. First, we found all candidate front-side halo CMEs within a 120-hour-long search window before the arrival time of the ICME-driven shock (or other upstream disturbance if there was no fully-developed shock, or the ICME arrival if there was no upstream disturbance). The 120-hour-long search window corresponds to a 1 AU transit speed of 347 km/s and is large enough to cover most possible CMEs sources except for extremely slow events. The large search window may produce several CME candidates, but further steps help to distinguish between likely and unlikely associations. The next step is to reduce the search window by estimating the CME transit time based on in-situ solar wind velocities at the location of shock arrival. Since fast CMEs tend to decelerate when moving through the slower solar wind, this method will give an upper estimate for the travel time. This method is not applicable to slow ICMEs because the corresponding, initially slow, CME may be accelerated by the ambient solar wind. In such cases, the full 120-hour window is used, and this may even be extended if the ICME of interest is extremely slow. The third step is that, for each remaining candidate CME in the search window, we consider whether the CME speed at the Sun is consistent with the 1 AU transit speed implied by an association with the 1 AU shock/ICME, and with the in-situ solar wind speed.

We recognize that the observed CME speed projected on the plane of the sky may not directly indicate the earthward-directed speed. Nevertheless, these speeds tend to be loosely correlated. Comparison with statistical studies of the relationship between CME speeds and 1 AU transit times, e.g. [*Cane et al.*, 2000; *Gopalswamy et al.*, 2000; *Zhang et al.*, 2003; *Xie et al.*, 2004; *Schwenn et al.*, 2005] can help to indicate whether a given CME-shock/ICME association is plausible or unlikely. We also take into consideration the solar source location implied by the CME/eruptive features. For example a central meridian source might be favored over a near-limb source, in particular if an ICME or magnetic cloud is involved in generating the storm. We should emphasize that the CME-ICME associations were considered by the working group members both individually (often using variations on the approach outlined above, and taking into account additional information, such as energetic particle observations which may link solar events and interplanetary shocks) and collectively, to arrive at a consensus.

We will use the storm on July 27, 2004 (Figure 2) as an example to illustrate the identification process. The solar wind speed at shock arrival is $\sim$ 900 km/s. If we simply assume that the CME-driven shock travels from the Sun at this constant speed, a travel time of $\sim$ 46 hour is implied, suggesting (since this is a "fast" event at 1 AU) an CME event after 00 UT, July 25 as the source. Examining the LASCO CME catalog as well as the related images, there was only one halo CME in the search window, at 14:54 UT on July 25. This had a high projected speed (1333 km/s) which was consistent with the fast ICME seen at Earth allowing for some deceleration in the inner heliosphere. A direct association can also be demonstrated for this event using energetic particle observations which show an increase commencing at the time of the CME [*Cane et al.*, 2006] that reaches peak intensity in the vicinity of the passage of the ICME-driven shock. This CME was associated with an M1.1 soft X-ray flare located at $N04°W30°$. The eruption at the surface was accompanied by a coronal dimming as shown in the running-difference EIT image (bottom middle panel of Figure 2). This CME/flare originated in NOAA AR 0652 as indicated in the MDI magnetogram (bottom left panel of Figure 2).

We should stress that it is not sufficient to use the time of the storm peak together with a plausible 1 AU transit time (e.g., based on the observed solar wind speeds at the time of the storm) to estimate the time of the solar source. Rather, it is important to examine and characterize the solar wind structures within which the geo-effective region is embeded, and then estimate the source timing. The effect of this distinction is illustrated by the event in Figure 2: the peak of the storm is ~ 16 hours after the arrival of the shock and ~ 12 hours after the arrival of the MC. These intervals are a significant fraction of the 1 AU transit times of the shock and ICME. Another point to note before leaving this event is that the two *Dst* minima in this storm result from two geo-effective regions, in the sheath and MC, associated with a single solar event. It therefor should not be assumed that multiple *Dst* minima within a storm interval indicate that multiple solar events are involved.

3.3. Storms Involving Complex Solar Wind structures and Multiple CMEs

We classify the solar-IP drivers of the major geomagnetic storms into three broad categories: S-type, M-type and C-type. S-type events are storms caused by single CMEs/ICMEs such as the July 24, 2004 storm described above. M-type are caused by multiple CMEs/ICMEs as discussed in this section. The C-type are for storms caused by CIRs [*Richardson et al.*, 2006]. For an M-type event, the storm is associated with complex solar wind structures that appear to involve multiple SHs and/or ICMEs. Two or more CMEs interact with each other in IP space, producing such complex flows [*Burlaga et al.*, 2002; *Zhang et al.*, 2003; *Wang et al.*, 2003]. Direct observations of the interaction between two CMEs near the Sun have been reported [*Gopalswamy et al.*, 2001]. The M-type events are treated as a separate category from S-type because of the apparent differences in terms of the propagation/arrival of ICMEs, the resulting IP structure and the geo-effective components.

One interesting variety of M-type events that we have noted is when a storm is generated by a faster ICME-driven shock propagating into the trailing edge of a slower ICME that originated in an earlier event at the Sun. An example is the storm of November 8, 1998 (Event 16, minimum $Dst = -149$ nT) shown in Figure 3. This storm was clearly generated by the region of southward magnetic field between 21 UT, November 7 and 05 UT, November 8. The ACE plasma and field data show a weak shock at 07:36 UT on November 7 followed by a probable ICME commencing at ~ 21 UT and indicated, for example, by the low proton temperature (black shading), enhanced magnetic field intensity, and enhancement in the solar wind O^7/O^6 ratio. The southward magnetic field in this structure generated the onset of the storm, reaching levels of $Dst \sim -100$ nT. A second, stronger shock, propagating through the ICME passed ACE at 04:21 UT on November 8. The magnetic field in the ICME was starting to turn toward the ecliptic at this time. However, the combination of the shock compression, which doubled the magnetic field strength and prevented the southward field strength from decaying, and the increase in solar wind speed, enhanced the y-component of the solar wind electric field, thereby strengthening storm activity and producing the peak of the storm. We suggest that ICME-associated plasma forms the post-shock sheath, at least to the end of the interval shown. Note that the field here turned northward, causing *Dst* to decline rapidly after the storm peak. We associate the shock on November 8 with a 1119 km/s halo CME with a source at $N22°W18°$ on November 5. Often in such situations, the source of the slower shock/ICME is less easily established. In the case of the shock on November 7, however, we suggest that a 523 km/s halo CME at 07:54 UT on November 4 originating from a quiet-Sun region associatd with a quiescent filament is a likely candidate. We classify this storm as M-type because, although the arrival of the November 8 shock is clearly associated with the peak of the storm, the presence of the southward fields in the preceding ICME is also required to generate the storm.

Before leaving this event, it is worth commenting on the chance juxtaposition of the November 8 shock, Earth and preceding ICME that generated the storm peak. Had the timing been slightly different, the storm peak strength could have been substantially different. For example, had the shock been delayed relative to the ICME by as little as an hour or so, it would have encountered a region of northward field. Hence, the shock-ICME interaction would not have contributed to the storm. If the shock had arrived an hour or two earlier, it would have encountered stronger southward fields in the ICME, and an even more intense storm might have been generated. This clearly illustrates that while for S-type events involving one CME, there may be some hope in the future of predicting the geoeffectiveness using solar observations to infer the CME magnetic field structure, a similar prediction is far more problematical for M-type events.

4. Results and Discussions

4.1. Table of Solar and IP Sources

Based on the methods described above, we have identified the solar and IP sources of the 88 major geomagnetic storms during 1996 – 2005. The results are summarized in Table 1. Columns 1 to 3 give the properties of each geomagnetic storm, as discussed earlier. In column 4, we list the overall solar-IP source type (S, M and C). Columns 5–10 describe the properties of solar source, and columns 11–14 the properties of the IP sources contributing to the geomagnetic activities. Column 15 indicates a (somewhat subjective) confidence level for our identifications, given as 1 to 3 in descending order of confidence. In the final column, "F" indicates that there are additional comments in a footnote. In many cases these summarize critical comments on the proposed associations or alternative proposals, from working group members.

Considering the properties of solar sources, the time in column 5 refers to the first appearance of CME in the LASCO C2 coronagraph, the CME velocity in column 6 refers to the average velocity of CME in the LASCO C2/C3 fields of view, and the angular width in column 7 is the apparent angular span of the CME in the plane of the sky measured in the C2 field of view. These values we generally obtained from the on-line LASCO CME catalog. However, in a few cases, they refer to previously unlisted CMEs that were identified from a re-examination of the LASCO images. Column 8 shows the magnitude of the soft X-ray flare associated with the source CME. Column 9 shows the surface source region type, whether an "AR" (active region) followed by the four digit NOAA AR number, "QS" (quiet sun region), or "CH" (coronal hole). Note that quiet Sun regions here refer to any region on the surface of the Sun outside the traditional active regions and coronal holes. As for the sources of CMEs, they are often associated with erupting quiescent filaments or filament channels.

Column 10 gives the heliographic coordinates of the surface source region. This generally corresponds to the H_α flare location reported by NOAA SEC. When no H_α flare location is reported, we used EIT images to measure the source coordinates, given by the location of the compact brightening, if observed, or the center of the dimming region if no brightening was observed. If the surface source regions of the CME candidates are unknown, because of the absence of any clear eruptive signatures on the disk in images from

EIT and other instruments, this is indicated by "UNK" in columns 9 and 10. For those events with LASCO/EIT data gaps, the solar source could still be identified in some cases (events 6, 13, 14, and 21) because a major long-duration solar flare occurred at an appropriate time (based on consideration of transit times and in-situ solar wind speeds, solar particle events, etc) and location. For these events, the time in column 5 is the flare onset time, followed by "(F)" to emphasize that this is not a CME time. Otherwise, "DG" in these columns indicates a gap in LASCO and/or EIT observations and that it was not possible to identify a probable source using alternative observations.

In the case of M-type events, there are multiple rows for each event listing the multiple CMEs that may contribute to the observed 1 AU solar wind structures. In each case, the first row indicates what we suggest is the "principal" solar driver. In the case of C-type events, the definitions of the parameters in the solar source columns are slightly different because of the different nature of the source. The time in column 5 indicates the central meridian transit time of the centroid of the associated coronal hole measured from EIT images. The time is followed by "(CH)" in order to emphasize that this does not refer to a CME source. The heliographic coordinate in column 10 indicates the latitude of coronal hole centroid when it crosses central meridian.

Considering the properties of IP sources, column 11 characterizes the solar wind components that contribute to the storm, while columns 12, 13 and 14 show the time of the CME-driven shock (or disturbance, at either ACE, indicated by "A", or WIND by "W"), and the start and ending times of the ICME. In column 11, We indicate in bold typeface the specific component(s) that contains the peak of the geomagnetic storm. Normal type indicates that the structure contributes to enhanced geomagnetic activity, but only to levels of > -100 nT. A plus sign indicates a simple succession of components, while a dash indicates an "interaction" between the components. For example, for event 3, a sheath and magnetic cloud contribute to the geomagnetic activity. The sheath does not drive *Dst* to major storm levels, while the magnetic cloud includes the peak of the major storm. In contrast in event 5, though the same structures are present, the sheath drives the peak of the storm. For M-type events, it can be difficult to summarize in a compact way, or even to identify unambiguously, the various components present, but the nature of the specific components driving the storm is indicated, e.g., "SH(M)" means the presence of a sheath-like region that may include features (such as additional shocks) that suggest that more than one solar/interplanetary event contributes. The situation where a shock is running into a preceding ICME or magnetic cloud, as discussed in relation to Figure 3 is indicated by PICME-SH or PMC-SH, respectively.

When identifying the solar sources, we have found that storms generated by a single slow ICME present a major challenge. In particular, it is perplexing that, for about 10 events (events 2,7, 28,31,34,36, 40, 58, 66, and 76 in Table 1), we were not able to find any halo CME candidates in the plausible search window with any apparent surface signatures (flare, filament eruption, dimming, brightening, or loop arcade), even though all the current solar disk observations, including EIT and SXT, were available. Similar "problem events" have been reported ealier [*Webb et al.*, 2000; *Zhang et al.*, 2003], and more recently, Schwenn et al. (2005) reported that about 20% of ICMEs observed at the Earth, regardless of the intensity of the resulting geomagnetic activity, were not preceded by an identifiable front-side halo CME (see also Cane and Richardson [2003]) Nevertheless, similar to the finding of Zhang et al. (2003), we could always (except for event 40) identify a slow halo CME that occurred 4 to 6 days before the arrival of the corresponding ICME and was consistent with the inferred transit times from the CME and ICME speeds. Since there were no surface signatures, these slow solar CMEs would conventionally be regarded as backside halo CMEs. However, one possibility, as suggested by Zhang et al.(2003), is that such slow CMEs could be from the front side but originate high in the corona, yielding little response in the low corona. In Table 1, we report such slow CMEs with unknown surface sources in columns 9 and 10. We emphasize that such reported CME sources are highly ambiguous, and caution must be exercised for further study of these events.

To give an idea of the confidence of the identifications, we have assigned for each event a confidence level (indicated in column 15 of Table 1). Levels 1, 2 and 3 indicate, with decreasing level of confidence, the most unambiguous, plausible, and ambiguous/uncertain identifications, respectively. For only 46 (52%) of the storms would we regard our associations as "level 1". These include most of the S-type and C-type events. The 27 (31%) level 2 storms include most M-type events and a few S-type. There are 15 (17%) events in level 3, including all the 10 problem events mentioned above. In the following sub-sections, we summarize the properties of the solar and IP sources listed in Table 1 and discuss their implications.

4.2. On the Types of Overall Solar-IP Sources

In Figure 4, we show the distribution of the three solar-IP source types for the 88 major geomagnetic storms during 1996 – 2005. The total numbers of S-type, M-type and C-type events are 53 (60%), 24 (27%), and 11 (13%), respectively. Hence, nearly two-thirds of these major storms were generated by single events at the Sun, and around another quarter involved multiple solar events. Considering S-type and M-type events together, we conclude that 77 ($\sim$ 87%) of the major storms in our study were driven by ICMEs (including the related upstream SH) and hence originated from eruptive solar events, the remainder being associated with CIRs and hence with coronal holes. This result agrees with previous studies that have concluded that major geomagnetic storms are predominantly caused by ICMEs and their related structures [*Gosling et al.*, 1991; *Tsurutani et al.*, 1997; *Richardson et al.*, 2001].

Nevertheless,, we also want to stress the non-trivial fraction ($\sim$ 13%) of these major geomagnetic storms that were driven by CIRs. Detailed analysis of these events (9 events from 1996 – 2004) has been reported by *Richardson et al.* [2006]. This is a somewhat surprising result but is also a consequence of the -100 nT *Dst* storm threshold chosen for the workshop – the strongest CIR-associated storm had a *Dst* minimum of -131 nT so all these events would have been excluded had a slightly lower *Dst* threshold been chosen. Furthermore, we note that three of the 88 major storms were generated by the interaction of a CIR with an ICME. These were events 22 (October 22, 1999; $Dst = -237$ nT), event 58 (October 1, 2002; $Dst = -176$ nT), and event 76 (August 30, 2004 ; $Dst = -126$ nT). These three events have been classified as S-type in the table because it is the presence of the ICME that is critical to the generation of the storm.

The year-by-year distribution of event types is shown in Figure 5. In 1996, the year of solar minimum, there was a single major storm driven by a CIR. Otherwise, during the rise, maximum and declining phases of cycle 23, the major storms were predominantly driven by ICMEs with S-type dominating over M-type. C-type events were observed in 1996 and 1998, were absent during 1999 – 2001 around solar maximum even though low latitude coronal holes and their associated streams were still typically present [*Luhmann et al.*, 2002], and reappeared in 2002 through 2005 during the declining phase of the cycle. The asymmetry in the number (3 versus 8) of CIR-generated storms between the rising and declining phase of the cycle, with more during the declining phase, has been noted in other studies [e.g., *Richardson et al.*, 2001]. Nevertheless, most major storms were still driven by ICMEs during 2002 – 2005.

For the 77 CME-driven storms events, around two thirds (53; 69%) were S-type and one third (24; 31%) M-type. The ratio of the numbers of S and M-type events does not show any clear solar cycle variation. Although we might expect M-type events to be more prominent at higher solar activity levels because of the higher CME rate, M-type events occurred throughout the solar rising, maximum and declining phases, except in 1997, when all 5 events were S-type, and S-type storms are still the most frequent type around solar maximum. The lack of a solar cycle dependence in the occurrence of M-type events may be due to the fact that, for at least half of the 24 M-type storms, the responsible multiple CMEs originated from the same active region rather than from separate solar source regions. Such "super" active regions may appear at any phase of the solar cycle.

4.3. On Geo-effective Solar Wind Components

Column 11 of Table 1 indicates that several configurations of IP structures gave rise to the major storms. For S-type events, the ICME and/or the upstream SH can contribute. We find that the storm peak was driven by the sheath in 12 of these events (22%), by an ICME that is a magnetic cloud in 30 events (57%) and by a non-cloud ICME in 11 events (21%). Hence, a majority of major storms involving a single CME/ICME were driven to storm maximum by a magnetic cloud. For the M-type events, the IP drivers are typically more complex, and involve multiple structures. Nevertheless, in most cases the storm driver can be characterized. In rare cases, such as event 10, a single driver among the various structures that pass the Earth (in this case a magnetic cloud) can be identified. A more common situation is that the storm peak is driven by a SH region or an ICME region that appears to include multiple components (indicated by SH(M) and ICME(M) respectively) that presumably reflect the complexity of the solar source. Multi-component SH region drive 9 storms and multi-component ICME or MC regions another 6 storms. The situation illustrated in Figure 3 in which a storm is caused by a shock propagating through a preceding ICME, drives the peak of 9 M-type storms, and hence is responsible for $\sim 10\%$ of all 88 major storms in this study.

Considering the 53 S-type and 24 M-type CME-driven storms together, the geo-effective components are MCs in 33 events (43%), ICMEs without clear cloud signatures account for another 14 events (18%), SH regions for 21 events (27%), and, as noted above, shocks propagating through preceding ICMEs/MCs in 9 events (12%). Hence, consistent with other studies, MCs form the most important class of IP drivers of major geomagnetic storms [*Wu and Lepping*, 2002; *Huttunen et al.*, 2005]. This is despite the fact that only a minority of ICMEs at Earth, in particular around solar maximum, have magnetic cloud signatures [*Richardson and Cane*, 2004]. The reason is that the magnetic fields associated with magnetic clouds can, if correctly oriented, provide the extended intervals of strong southward field that drive major storms, such as in Figure 2. Other ICMEs typically have less organized, more irregular magnetic fields that may also be less enhanced, and hence non-cloud ICMEs are typically less geoeffective. Nevertheless, even if a magnetic cloud is present, it may not drive the peak of the storm if the cloud field orientation is not conducive for storm generation. For example, in event 5, it is the sheath ahead of the magnetic cloud that drives the peak of the storm. More than half of the major storms are associated with other structures which have less organized magnetic structure, and hence in principle have less "predictable" geomagnetic consequences [*Huttunen and Koskinen*, 2004].

4.4. On Solar CMEs Associated with Major Geomagnetic Storms

Except for the $\sim 10\%$ of events driven by CIRs, all the other major geomagnetic storms in our survey were caused by IP transients following solar CMEs. After excluding events that occurred during LASCO data gaps, we were able to identify 68 CMEs that were the likely solar sources of these storms, as given in Table 1. Apparently, these 68 CMEs are the most effective in producing geomagnetic storms among thousands of CMEs observed during 1996 – 2005. When summarizing the properties of these CMEs, only the presumed "principle" CME (shown as the first CME in the list of possible multiple sources in the event table) is included for M-type events.

Considering the apparent angular size of these CMEs, 46 (68%) were full halo CMEs, and 22 (32%) were partial halo CMEs. Clearly, partial halo CMEs should be considered when searching for the solar drivers of major geomagnetic storms. During the same period, LASCO observed 1187 halo CMEs of which 378 (32%) were full halos, and 809 (68%) were partial halos. Comparing with the number of similar CMEs that produced major storms, we estimate that about one out of eight full halo CMEs (or one quarter of front-side full halo CMEs, assuming that around half of halo CMEs originate on the backside of the Sun) will cause a major geomagnetic storm, and about 1 in 36 partial halo CMEs will do. If all LASCO CMEs, 10410 in total in the period of interest, are considered, on average only 1 out of ~ 150 CMEs will cause a major storm. Since halo CMEs comprises only a small fraction of all CMEs observed, it is practical to use these relatively rare events to predict the interception of an ICME by the Earth, and hence the possible generation of a geomagnetic storm. However, these is certainly not a one-to-one association between halo CMEs and ICMEs at Earth. About 15% front-side halo CMEs may not intercept the Earth, and some 20% of ICMEs are not preceded by identifiable front-side halo CMEs [*Schwenn et al.*, 2005] Furthermore, when an ICME does intercept the Earth, the magnetic field configuration still has to be conducive for the generation of a major storm. The ICME rate at Earth [*Cane and Richardson*, 2003], far exceeds the rate of major storms, for example by a factor of ~ 4 around solar maximum.

In Figure 6, we display the speed distribution of the 68 CMEs associated with major geomagnetic storms. Remarkably, the distribution has a wide range from ~ 60 km/s to $\sim$2800 km/s with evidence of a peak at about 900 km/s. The average (median) speed of the 68 CMEs is 945 km/s (875 km/s). A similar average speed (855 km/s) was obtained by *Gopalswamy* [2006] for a set of 55 geoeffective CMEs. For comparison, the average (median) speed of all 10410 CMEs in the study period is 472 km/s (410 km/s), and the average (median) speed of all 1187 halo CMEs is 767 km/s (636 km/s). Hence, the major storm-associated CMEs are on average around twice as fast as the all-CME average, in agreement with recent results [*Webb*, 2002; *Yashiro et al.*, 2004]. Forty-five (66%) of the 68 major storm-associated CMEs have speeds in the LASCO C2/C3 fields of view that exceed 600 km/s. These properties are consistent with the expectation that major geomagnetic storms are usually due to fast halo CMEs.

Nevertheless, the relatively small (~ 200 km/s) difference between the average speeds for all halo CMEs and major storm-associated CMEs suggests that strongly geo-effective halo CMEs cannot necessarily be distinguished from other halo CMEs on the basis of their speed alone, as discussed earlier by *Zhang et al.* [2003]. Further, some very slow CMEs, though a small faction, can also generate major storms. Twelve (18%) of the 68 storm-associated CMEs had speeds of less than 300 km/s. These results emphasize the fact that speed alone is not the major factor determining geoeffectiveness. Rather, the configuration of the embedded magnetic fields is also important, as exemplified by the fact that most of these storms resulted from slow magnetic clouds at the Earth with speeds comparable to the ambient solar wind.

Considering the association of major storms with GOES soft X-ray flares, we find that among the 77 CME-driven storms, 19 (25%) were associated with a X-class flare, 17 (22%) with a M-class flare, 19 (25%) with a C-class flare, and 22 (28%) with either minor (B or A-class), or with no evidence of a flare. We conclude that, major (M or X-class) flares were associated with about one half of our major storms, and that around a third of the storms were not accompanied by a flare or only by a minor flare. Therefore using flares, the traditional indicator of solar activity, to predict geomagnetic storms is often far from satisfactory [*Gosling*, 1993].

4.5. On the Solar Surface Source Regions Associated with Major Geomagnetic Storms

Figure 7 summarizes nature of the solar surface source regions where the major storms in our study originated (Column 9 of Table 1). For 3 of the 88 events, there were insufficient data (e.g., data gap in LASCO/EIT observations, and no major flares reported in a plausible time window) for the source to be inferred. In the case of M-type events, we only include the source of the principle CME. We find that 54 storms ($\sim$ 63%) originated in active regions, 10 (12%) in quiet Sun regions, and 11 (13%) were associated with coronal holes. Here, quiet Sun region is a general reference to any coronal region other than active regions or coronal holes. It should be noted though that even when a CME originates outside an active region, it is usually associated with a quiescent filament or filament channel overlying a magnetic inversion line in the photosphere. For the remaining 10 (12%) events we were unable to identify any solar surface signature and hence the nature of the source region is unknown.

Thus, while half of the major geomagnetic storms originated in active regions, a similar number originated outside active regions. Nevertheless, active regions remain the source of the largest storms. The ten largest storms (minimum Dst $\leq$ -271 nT) during 1996 – 2005 were all associated with active regions. For comparison, the largest storm that originated from a quiet Sun region reached $Dst = -237$ nT. Furthermore, the largest storm with an unknown surface source attained $Dst = -182$ nT, and the largest storm from a coronal hole source had a minimum Dst of only -131 nT.

In Figure 8, we show the heliographic distribution of the source regions (Column 10 of Table 1). This distribution includes the 64 CMEs with identified surface sources. The other 24 events are excluded because they were associated with coronal holes (11 events), or unidentified sources (10 events), or occurred within solar data gaps (3 events). The source locations lie within 35°N to 58°S latitude both for active region (red symbols) and quiet Sun sources (blue symbols), and 61 of the 64 source regions (95%) lie within 30° from central meridian. A possible explanation is that CMEs originating from higher latitudes propagate into the high latitude region of the heliosphere and do not intercept the Earth.

Considering the longitudinal distribution, 56 of the 64 source regions (88%) lie within 45° from central meridian, (77%) within 30°, and 34 (53%) within 15°. Hence, the vast majority of major storms arise from solar sources that are close to central meridian. Nevertheless, the sources also show an east-west asymmetry that favors the western hemisphere and reinforces the similar result from the study of *Zhang et al.* [2003]. Specifically, the sources extend to 85°W, but only to 58°E, and 42 lie on the western hemisphere, compared with 21 on the eastern hemisphere (one event is at central meridian). Hence, the ratio of number of western to eastern sources is $\sim$2:1. The average (median) longitude of all the 64 events studied is 11°W (8°W). Geo-effective CMEs could be from far western regions but not from far eastern regions. This east-west asymmetry seems to be a general feature of the ICMEs that intercept the Earth, regardless the strength of geo-activity [*Wang et al.*, 2002; *Cane and Richardson*, 2003]. One possible explanation is that this asymmetry results from the deflection of CME trajectories by the spiral IP magnetic field [*Wang et al.*, 2004].

4.6. Implication for Forecasting Major Geomagnetic Storms

What are the implications of this study for forecasting major geomagnetic storms using solar observations? First, there may be a misconception that a major geomagnetic storm must be caused by an unusually fast halo CME from a strong active region accompanied by various energetic eruptive signatures (e.g., major solar flares). Except for a few super storms, this was not the case for many of the major storms ($Dst \leq -100$ nT). In fact, some of these storms were caused by moderate speed CMEs that may originate outside of active regions, as well as by CIRs associated with coronal holes as described earlier. A central reason is that the driving electric field y-component depends on both the solar wind speed and B_s, but the dynamic range of B_s is greater than that of the solar wind speed. However, a combination of CME speed and magnetic field in ICMEs seem to have a high correlation with Dst index [*Gopalswamy*, 2006]. Furthermore, activity is suppressed when the IMF is northward, so a fast ICME with a predominantly strong northward field will not generate a major storm. The size of a storm also depends on the time variation of the southward field component. Thus, a relatively slow moving MC with an extended region of enhanced southward field (such as event 15) can generate a major storm. Hence, the speed of a halo CME alone is an inconsistent predictor of a major geomagnetic storm. A major advance would be able to "predict" the interplanetary magnetic field configuration at 1 AU, in particular for S-type storms involving only one CME/ICME, based on solar observations, but this is difficult at present.

In the case of storms that involve more than one CME/ICME, a complicating factor for forecasting is that it is the details of the magnetic structures formed by the interaction of these transients (and their associated shocks), both with each other and with the ambient solar wind, that determine the resulting level of geomagnetic activity. The precise path of the Earth through the structure is also a factor. Thus, it is unlikely that even a relatively complete MHD simulation of two CMEs launched towards the Earth would ever include sufficient information to be able to model the resulting fields at 1 AU on the necessary few-hour timescales. Information from upstream spacecraft would help to assess the likely geomagnetic impact, but the interacting structures may still evolve before reaching Earth.

5. Summary

We have investigated the solar and IP sources of the 88 major geomagnetic storms ($Dst \leq -100$ nT) that occurred during 1996 – 2005 with the aim of providing a reliable as possible list of associations that is intended to provide a basis of future studies by the LWS CDAW participants and others. By combining remote-sensing solar observations, in-situ near-Earth solar wind observations, and the wide range of experience of the Working Group members, we were able to identify with reasonable confidence the chain of sources for about 83% (73) of these events, although the detailed one-to-one association could not be established for those complex events involving multiple CMEs and ICMEs. We are uncertain of the origin of the other 17% (15) of the storms, mainly because their driving CMEs were not associated with noticeable eruption signatures at the solar surface. Detailed parameters of the solar and IP sources for each of the 88 major geomagnetic storms have been provided. The main results are as follows:

(1) Based on the overall solar and IP properties, the sources can be divided into three broad categories: S-type, driven by single CMEs and thier IP counterparts; M-type, associated with multiple CMEs/ICMEs, and C-type due to CIRs driven by high speed streams from coronal holes. The total numbers of S-type, M-type and C-type events are 53 (60%), 24 (27%), and 11 (13%), respectively.

(2) Of the 68 LASCO CMEs associated with these major storms, 46 (68%) were full halo CMEs, and 22 (32%) were partial halo CMEs. Their speed have a wide range (60 km/s to 2800 km/s). The average speed (945 km/s) is about twice as fast as the average for all LASCO CMEs. About half (47%) of these storm-associated CMEs were accompanied by major (X and M-class) flares.

(3) For the 85 storms for which we could identify the solar surface source, we find that 54 ($\sim$ 63%) originated in active regions, 10 (12%) in quiet Sun regions associated with quiescent filaments, and 11 (13%) were associated with coronal holes. The other 10 (12%) events originated from unknown surface source regions.

(4) Major geomagnetic storms predominantly originate from sources near central meridian (e.g., 88% from with 45°, and 77% from with 30° of central meridian) but show an east-west asymmetry with around twice as many storms originating on the western hemisphere than on the eastern hemisphere.

Acknowledgments.

We acknowledge the many researchers who have contributed to the data used in this study. In particular, the ACE plasma, magnetic field and composition/charge state data were provided by the ACE Science Center. SOHO is a project of international cooperation between ESA and NASA. The LASCO instrument was constructed by a consortium of the Naval Research Laboratory, University of Birmingham (England), the Max-Planck-Institute für Aeronomie (Germany) and the Laboratoire d'Astronomie Spatiale (France). We acknowledge the usage of the CME catalog generated and maintained at the CDAW Data Center by NASA and The Catholic University of America in cooperation with the Naval Research Laboratory. Travel support to some participants to the CDAW workshop is provided by NASA's LWS TR&T program. J. Zhang is supported by NASA grants NNG04GN36G, NNG05GG19G and NSF SHINE grant ATM-0454612. DFW was supported by AFRL contracts AF19628-00-C-0073 and FA8718-04-C-0050. A. N. Z. acknowledge support from the Belgian Federal Science Policy Office through the ESA-PRODEX programme.

References

Berdichevsky, D. B., C. J. Farrugia, B. J. Thompson, R. P. Lepping, D. V. Reames, M. L. Kaiser, J. T. Steinberg, S. P. Plunkett, and D. J. Michels, Halo-coronal mass ejections near the 23rd solar minimum: lift-off, inner heliosphere, and in situ (1 AU) signatures, *Annales Geophysicae*, *20*, 891–916, 2002.

Brueckner, G. E., R. A. Howard, M. J. Koomen, C. M. Korendyke, D. J. Michels, J. D. Moses, D. G. Socker, K. P. Dere, P. L. Lamy, A. Llebaria, M. V. Bout, R. Schwenn, G. M. Simnett, D. K. Bedford, and C. J. Eyles, The large angle spectroscopic coronagraph (LASCO), *Sol. Phys.*, *162*, 357–402, 1995.

Brueckner, G. E., J.-P. Delaboudiniere, R. A. Howard, S. E. Paswaters, O. C. St. Cyr, R. Schwenn, P. Lamy, G. M. Simnett, B. Thompson, and D. Wang, Geomagnetic storms caused by coronal mass ejections (CMEs): March 1996 through June 1997, *Geophys. Res. Lett.*, *25*, 3019, 1998.

Burlaga, L. F., S. P. Plunkett, and O. C. St. Cyr, Successive CMEs and complex ejecta, *J. Geophys. Res.*, *107*, 1266, doi:10.1029/2001JA000,255, 2002.

Cane, H. V., and I. G. Richardson, Interplanetary coronal mass ejections in the near-earth solar wind during 1996–2002, *J. Geophys. Res.*, *108(A4)*, 1156, doi:10.1029/2002JA009,817, 2003.

Cane, H. V., I. G. Richardson, and O. C. St. Cyr, Coronal mass ejections, interplanetary ejecta and geomagnetic storms, *Geophys. Res. Lett.*, *27*, 3591–3594, 2000.

Cane, H. V., R. A. Mewaldt, C. M. S. Cohen, and T. T. von Rosenvinge, Role of flares and shocks in determining solar energetic particle abundances, *Journal of Geophysical Research (Space Physics)*, *111*(A10), 6, doi:10.1029/2005JA011071, 2006.

Cliver, E. W., Y. Kamide, and A. G. Ling, The semiannual variation of geomagnetic activity: phases and profiles for 130 years of /aa data, *Journal of Atmospheric and Terrestrial Physics*, *64*, 47–53, 2002.

Crooker, N. U., E. W. Cliver, and B. T. Tsurutani, The semiannual variation of great geomagnetic storms and the postshock Russell-Mcpherron effect preceding coronal mass ejecta, *Geophys. Res. Lett.*, *19*, 429–432, 1992.

Delaboudiniere, J.-P., G. E. Artzner, J. Brunaud, and et al., EIT: Extreme-ultraviolet imaging telescope for the SOHO mission, *Sol. Phys.*, *162*, 291–312, 1995.

Dungey, J. R., Interplanetary magnetic field and auroral zones, *Phys. Rev. Lett.*, *6*, 47, 1961.

Forsyth, R. J., and E. Marsch, Solar Origin and Interplanetary Evolution of Stream Interfaces, *Space Science Reviews*, *89*, 7–20, doi:10.1023/A:1005235626013, 1999.

Gonzalez, W. D., J. A. Joselyn, Y. Kamide, H. W. Kroehl, G. Rostoker, B. T. Tsurutani, and V. M. Vasyliunas, What is a geomagnetic storm?, *J. Geophys. Res.*, *99*, 5771, 1994.

Gopalswamy, N., Coronal Mass Ejections of Solar Cycle 23, *Journal of Astrophysics and Astronomy*, *27*, 243–254, 2006.

Gopalswamy, N., A. Lara, R. P. Lepping, M. L. Kaiser, D. Berdichevsky, and O. C. St. Cyr, Interplanetary acceleration of coronal mass ejections, *Geophys. Res. Lett.*, *27*, 145–148, 2000.

Gopalswamy, N., S. Yashiro, M. L. Kaiser, R. A. Howard, and J. L. Bougeret, Radio signatures of coronal mass ejection interaction: Coronal mass ejection cannibalism?, *Astrophys. J.*, *548*, L91–L94, 2001.

Gopalswamy, N., S. Yashiro, G. Michalek, H. Xie, R. P. Lepping, and R. A. Howard, Solar source of the largest geomagnetic storm of cycle 23, *Geophys. Res. Lett.*, *32*, L12S09, doi:10.1029/2004GL021,639, 2005.

Gosling, J. T., The solar flare myth, *J. Geophys. Res.*, *98(A11)*, 18,937, 1993.

Gosling, J. T., and D. J. McComas, Field line draping about fast coronal mass ejecta - A source of strong out-of-the-ecliptic interplanetary magnetic fields, *Geophys. Res. Lett.*, *14*, 355–358, 1987.

Gosling, J. T., D. J. McComas, J. L. Phillips, and S. J. Bame, Geomagnetic activity associated with earth passage of interplanetary shock disturbances and coronal mass ejections, *J. Geophys. Res.*, *96*, 7831–7839, 1991.

Hill, S. M., V. J. Pizzo, C. C. Balch, D. A. Biesecker, P. Bornmann, E. Hildner, L. D. Lewis, R. N. Grubb, M. P. Husler, K. Prendergast, J. Vickroy, S. Greer, T. Defoor, D. C. Wilkinson, R. Hooker, P. Mulligan, E. Chipman, H. Bysal, J. P. Douglas, R. Reynolds, J. M. Davis, K. S. Wallace, K. Russell, K. Freestone, D. Bagdigian, T. Page, S. Kerns, R. Hoffman, S. A. Cauffman, M. A. Davis, R. Studer, F. E. Berthiaume, T. T. Saha, G. D. Berthiume, H. Farthing, and F. Zimmermann, The NOAA Goes-12 Solar X-Ray Imager (SXI) 1. Instrument, Operations, and Data, *Sol. Phys.*, *226*, 255–281, doi:10.1007/s11207-005-7416-x, 2005.

Howard, R. A., D. J. Michels, N. R. Sheeley, Jr., and M. J. Koomen, The observation of a coronal transient directed at earth, *Astrophys. J.*, *263*, L101–L104, 1982.

Huttunen, K., and H. Koskinen, Importance of post-shock streams and sheath region as drivers of intense magnetospheric storms and high-latitude activity, *Annales Geophysicae*, *22*, 1729–1738, 2004.

Huttunen, K. E. J., R. Schwenn, V. Bothmer, and H. E. J. Koskinen, Properties and geoeffectiveness of magnetic clouds in the rising, maximum and early declining phases of solar cycle 23, *Annales Geophysicae*, *23*, 625–641, 2005.

Jackson, B. V., A. Buffington, P. P. Hick, R. C. Altrock, S. Figueroa, P. E. Holladay, J. C. Johnston, S. W. Kahler, J. B. Mozer, S. Price, R. R. Radick, R. Sagalyn, D. Sinclair, G. M. Simnett, C. J. Eyles, M. P. Cooke, S. J. Tappin, T. Kuchar, D. Mizuno, D. F. Webb, P. A. Anderson, S. L. Keil, R. E. Gold, and N. R. Waltham, The Solar Mass-Ejection Imager (SMEI) Mission, *Sol. Phys.*, *225*, 177–207, doi:10.1007/s11207-004-2766-3, 2004.

Klein, L. W., and L. F. Burlaga, Interplanetary magnetic clouds at 1 AU, *J. Geophys. Res.*, *87*, 613–624, 1982.

Lepping, R. P., C.-C. Wu, and D. B. Berdichevsky, Automatic identification of magnetic clouds and cloud-like regions at 1 AU: occurrence rate and other properties, *Annales Geophysicae*, *23*, 2687–2704, 2005.

Lepri, S. T., T. H. Zurbuchen, L. A. Fisk, I. G. Richardson, H. V. Cane, and G. Gloeckler, Iron charge distribution as an identifier of interplanetary coronal mass ejections, *J. Geophys. Res.*, *106*, 29,231–29,238, doi:10.1029/2001JA000014, 2001.

Lindsay, G. M., J. G. Luhmann, C. T. Russell, and J. T. Gosling, Relationships between coronal mass ejection speeds from coronagraph images and interplanetary characteristics of associated interplanetary coronal mass ejections, *J. Geophys. Res.*, *104*, 12,515, 1999.

Luhmann, J. G., Y. Li, C. N. Arge, P. R. Gazis, and R. Ulrich, Solar cycle changes in coronal holes and space weather cycles, *Journal of Geophysical Research (Space Physics)*, *107*, 3–1, doi:10.1029/2001JA007550, 2002.

Neugebauer, M., and R. Goldstein, Particle and field signatures of coronal mass ejections in the solar wind, in *Coronal Mass Ejections*, edited by N. Crooker, J. A. Joselyn, and J. Feynman, Geophys. Monogr. ser. 99, pp. 245–251, AGU, Washington D. C., 1997.

O'Brien, T. P., and R. L. McPherron, An empirical phase space analysis of ring current dynamics: Solar wind control of injection and decay, *J. Geophys. Res.*, *105(A4)*, 7707–7719, 2000.

Perreault, P., and S.-I. Akasofu, A study of geomagnetic storms, *Geophys. J.*, *54*, 547, 1978.

Richardson, I. G., and H. V. Cane, Regions of abnormally low proton temperature in the solar wind (1965-1991) and their association with ejecta, *J. Geophys. Res.*, *100*, 23,397–23,412, doi:10.1029/95JA02684, 1995.

Richardson, I. G., and H. V. Cane, The fraction of interplanetary coronal mass ejections that are magentic clouds: Evidence for a solar cycle variation, *Geophys. Res. Lett.*, *31*, L18,804, 2004.

Richardson, I. G., E. W. Cliver, and H. V. Cane, Sources of geomagnetic storms for solar minimum and maximum conditions during 1972-2000, *Geophys. Res. Lett.*, *28*, 2569–2572, doi: 10.1029/2001GL013052, 2001.

Richardson, I. G., H. V. Cane, and E. W. Cliver, Sources of geomagnetic activity during nearly three solar cycles (1972–2000), *J. Geophys. Res.*, *107(A8)*, doi:10.1029/2001JA000,504, 2002.

Richardson, I. G., D. F. Webb, J. Zhang, D. B. Berdichevsky, D. A. Biesecker, J. C. Kasper, R. Kataoka, J. T. Steinberg, B. J. Thompson, C.-C. Wu, and A. N. Zhukov, Major geomagnetic storms (Dst $\leq$ -100 nT) generated by corotating interaction regions, *Journal of Geophysical Research (Space Physics)*, *111*(A10), 7, doi:10.1029/2005JA011476, 2006.

Russell, C. T., and R. L. McPherron, Semiannual variation of geomagnetic activities, *J. Geophys. Res.*, *78*, 1105, 1973.

Scherrer, P. H., R. S. Bogart, R. I. Bush, J. T. Hoeksema, A. G. Kosovichev, J. Schou, W. Rosenberg, L. Springer, T. D. Tarbell, A. Title, C. J. Wolfson, I. Zayer, and MDI Engineering Team, The Solar Oscillations Investigation - Michelson Doppler Imager, *soph*, *162*, 129–188, 1995.

Schwenn, R., A. Dal Lago, E. Huttunen, and W. D. Gonzalez, The association of coronal mass ejections with their effects near the earth, *Annales Geophysicae*, *23(3)*, 1033–1059, 2005.

Thompson, B. J., S. P. Plunkett, J. B. Gurman, J. S. Newmark, O. C. St. Cyr, and D. J. Michels, SOHO/EIT observations of an earth-directed coronal mass ejection on May 12, 1997, *Geophys. Res. Lett.*, *25*, 2465, 1998.

Tsuneta, S., L. Acton, M. Bruner, J. Lemen, W. Brown, R. Caravalho, R. Catura, S. Freeland, B. Jurcevich, and J. Owens, The soft X-ray telescope for the SOLAR-A mission, *Sol. Phys.*, *136*, 37–67, 1991.

Tsurutani, B. T., and W. D. Gonzalez, The interplanetary causes of magnetic storms: A review, in *Magnetic Storms*, edited by B. T. Tsurutani, W. D. Gonzalez, Y. Kamide, and J. K. Arballo, Geophys. Monogr. Ser. 98, p. 77, AGU, 1997.

Tsurutani, B. T., W. D. Gonzalez, Y. Kamide, and J. K. Arballo (Eds.), *Magnetic storms*, Geophys. Monogr. ser. 98, AGU, Washington, D. C., 1997.

Tsurutani, B. T., W. D. Gonzalez, A. L. C. Gonzalez, F. L. Guarnieri, N. Gopalswamy, M. Grande, Y. Kamide, Y. Kasahara, G. Lu, I. Mann, R. McPherron, F. Soraas, and V. Vasyliunas, Corotating solar wind streams and recurrent geomagnetic activity: A review, *Journal of Geophysical Research (Space Physics)*, *111*(A10), 7, doi:10.1029/2005JA011273, 2006.

Wang, Y., C. Shen, P. Ye, and S. Wang, Deflection of coronal mass ejection in the interplanetary medium, *Sol. Phys.*, *222*, 329–343, 2004.

Wang, Y. M., P. Z. Ye, S. Wang, G. P. Zhou, and J. X. Wang, A statistical study on the geoeffectiveness of earth-directed coronal mass ejections from March 1997 to December 2000, *J. Geophys. Res.*, *107(A11)*, 1340, doi:10.1029/2002JA009,244, 2002.

Wang, Y. M., P. Z. Ye, and S. Wang, Multiple magnetic clouds: Several examples during March – April, 2001, *J. Geophys. Res.*, *108(A10)*, 1370, doi:10.1029/2003JA009,850, 2003.

Webb, D. F., CMEs and the solar cycle variation in their geoeffectiveness, in *ESA SP-508: From Solar Min to Max: Half a Solar Cycle with SOHO*, edited by A. Wilson, pp. 409–419, 2002.

Webb, D. F., E. W. Cliver, N. U. Crooker, O. C. St. Cyr, and B. J. Thompson, Relationship of halo coronal mass ejections, magnetic clouds, and magnetic storms, *J. Geophys. Res.*, *105(A4)*, 7491–7508, 2000.

Webb, D. F., N. U. Crooker, S. P. Plunkett, and O. C. St. Cyr, The solar sources of geoeffective structures, in *Space Weather*, edited by S. Paul, J. S. Howard, and L. S. George, Geophys. Monogr. Ser. 125, pp. 123–142, AGU, 2001.

Webb, D. F., D. R. Mizuno, A. Buffington, M. P. Cooke, C. J. Eyles, C. D. Fry, L. C. Gentile, P. P. Hick, P. E. Holladay, T. A. Howard, J. G. Hewitt, B. V. Jackson, J. C. Johnston, T. A. Kuchar, J. B. Mozer, S. Price, R. R. Radick, G. M. Simnett, and S. J. Tappin, Solar Mass Ejection Imager (SMEI) observations of coronal mass ejections (CMEs) in the heliosphere, *Journal of Geophysical Research (Space Physics)*, *111*(A10), 12,101, doi:10.1029/2006JA011655, 2006.

Wimmer-Schweingruber, R. F., N. U. Crooker, A. Balogh, V. Bothmer, R. J. Forsyth, P. Gazis, J. T. Gosling, T. Horbury, A. Kilchenmann, I. G. Richardson, J. D. Richardson, P. Riley, L. Rodriguez, R. V. Steiger, P. Wurz, and T. H. Zurbuchen, Understanding Interplanetary Coronal Mass Ejection Signatures, *Space Science Reviews*, *123*, 177–216, doi: 10.1007/s11214-006-9017-x, 2006.

Wu, C.-C., and R. P. Lepping, Effects of magnetic clouds on the occurrence of geomagnetic storms: The first 4 years of Wind, *J. Geophys. Res.*, *107(A10)*, 1314, doi:10.1029/2001JA000,161, 2002.

Xie, H., L. Ofman, and G. Lawrence, Cone model for halo cmes: Application to space weather forecasting, *J. Geophys. Res.*, *109*, A03,109, 2004.

Yashiro, S., N. Gopalswamy, G. Michalek, O. C. St. Cyr, S. P. Plunkett, N. B. Rich, and R. A. Howard, A catalog of white light coronal mass ejections observed by the SOHO spacecraft, *Journal of Geophysical Research (Space Physics)*, *109*(A18), 7105, doi:10.1029/2003JA010282, 2004.

Zhang, J., K. P. Dere, R. A. Howard, and V. Bothmer, Identification of solar sources of major geomagnetic storms between 1996 and 2000, *Astrophys. J.*, *582*, 520–533, 2003.

Zurbuchen, T. H., and I. G. Richardson, In-Situ Solar Wind and Magnetic Field Signatures of Interplanetary Coronal Mass Ejections, *Space Science Reviews*, *123*, 31–43, doi: 10.1007/s11214-006-9010-4, 2006.

J. Zhang, Department of Computational and Data Sciences, George Mason University, 4400 University Dr., MSN 6A2, Fairfax, VA 22030, USA. (jzhang7@gmu.edu)

I. G. Richardson, Code 661, NASA Goddard Space Flight Center Greenbelt, MD 20771, USA. (ian.richardson@gsfc.nasa.gov)

D. F. Webb, Boston College, Inst. for Scientific Research, 140 Commonwealth Ave., Chestnut Hill, MA 02467, USA. (david.webb.ctr@hanscom.af.mil)

N. Gopalswamy, Solar System Exploration, Code 695 NASA Goddard Space Flight Center Greenbelt, MD 20771, USA. (gopals@ssedmail.gsfc.nasa.gov)

E. Huttunen, University of California, Berkeley, Space Sciences Laboratory 7 Gauss Way 7450, Berkeley, CA 94720-7450,USA. (huttunen@ssl.berkeley.edu)

J. Kasper, MIT Center for Space Research, 77 Massachusetts Ave., Cambridge, MA 02139, USA. (jck@mit.edu)

N. V. Nitta, LMSAL, B/252, Dept/ADBS, 3251 Hanover Street, Palo Alto, CA 94304, USA. (nitta@lmsal.com)

W., Poomvises Department of Computational and Data Sciences, George Mason University, 4400 University Dr., MSN 6A2, Fairfax, VA 22030, USA. (wpoomvis@gmu.edu)

B. J., Thompson, Code 612, NASA Goddard Space Flight Center Greenbelt, MD 20771, USA. (barbara.j.thompson@nasa.gov)

C.-C., Wu, Code 696, NASA Goddard Space Flight Center Greenbelt, MD 20771, USA. (wuc@cspar.uah.edu)

S., Yashiro, Solar System Exploration, Code 695 NASA Goddard Space Flight Center Greenbelt, MD 20771, USA. (yashiro@ssedmail.gsfc.nasa.gov)

A. N.Zhukov, Royal Observotary of Belgium, Avenue Circulaire 3, B-1180 Brussels, Belgium (Andrei.Zhukov@oma.be)

Solar and Interplanetary Sources of the 78 Major Geomagnetic Storms during 1996–2004

1	2	3	4	5	6	7	8	9	10	11	12	13	14	15	16
ID[a]	Dst (min)		S-IP[b]	CME			Flare	Source[d]	Source[e]	IP Solar Wind[f]	Shock[g]	ICME		CL[h]	FN[i]
	Time (UT)	Int. (nT)	Driver (Type)	Time[c] (UT)	Vel km/s	AW (d)	Class	Region (Type)	Coord.	Structure (Type)	Time (UT)	Start (UT)	End UT		
1	1996/10/23 05	-105	C	10/20 07:03(CH)	..	..	..	CH	S10	**CIR**	..	..	..	1	
2	1997/04/22 00	-107	S	04/16 07:35	87	113	NO	UNK	UNK	**MC**	04/21 06	04/21 10	04/23 04	3	F
3	1997/05/15 13	-115	S	05/12 05:30	464	360	C1.3	AR8038	N21W08	SH+**MC**	05/15 01:15(W)	05/15 09	05/16 00	1	
4	1997/10/11 04	-130	S	10/06 15:28	293	174	NO	QS	S27W05	SH+**MC**	10/10 15:57(W)	10/10 22	10/12 00	1	F
5	1997/11/07 05	-110	S	11/04 06:10	785	360	X2.1	AR8100	S14W33	**SH**+MC	11/06 22:02(A)	11/07 04	11/08 10	1	
6	1997/11/23 07	-108	S	11/19 17:00(F)	..	..	C1.6	AR8108	N20E05	SH+**MC**	11/22 09:12(W)	11/22 18	11/23 14	2	F
7	1998/02/18 01	-100	S	02/12 15:55	63	126	No	UNK	UNK	**MC**	02/17 04	02/17 10	02/17 21	3	F
8	1998/03/10 21	-116	C	03/08 09:03(CH)	..	..	NO	CH	S30	**CIR**	..	..	..	1	
9	1998/05/04 06	-205	M	05/02 14:06	938	360	X1.1	AR8210	S15W15	**PICME-SH**	05/04 02:15(A)	..	..	2	F
			..	05/02 05:31	542	360	C5.4	AR8210	S19W09	..	..	..	..	..	
			..	05/01 23:40	585	360	M1.2	AR8210	S18W04	..	..	..	..	..	
			..	04/29 16:59	1374	360	M6.8	AR8210	S18E20	..	05/01 21:21(W)	05/02 05	05/04 02	..	
10	1998/06/26 05	-101	M	06/22 07:34	289	119	NO	QS	S58W05	**MC**	06/25 15:43(A)	06/25 23	06/26 19	2	F
			..	06/21 05:35	192	163	NO	AR8243	N15W30	..	06/24 10	06/24 16	06/25 23	..	
11	1998/08/06 12	-138	M	DG	..	..	NO	DG	DG	**PICME-SH**	08/06 07:16(W)	08/05 13	08/06 12	3	F
12	1998/08/07 06	-108	C	DG	..	..	NO	CH	DG	**CIR**	..	..	..	2	F
13	1998/08/27 10	-155	S	08/24 21:50(F)	..	..	X1.0	AR8307	N35E09	SH+**ICME**	08/26 06:40(W)	08/26 22	08/28 00	1	F
14	1998/09/25 10	-207	S	09/23 06:40(F)	..	..	M7.1	AR8340	N18E09	SH+**MC**	09/24 23:20(W)	09/25 02	09/26 16	1	F
15	1998/10/19 16	-112	S	10/15 10:04	362	360	NO	QS	N10E10	SH+**MC**	10/18 19:00(A)	10/19 04	10/20 07	1	F
16	1998/11/08 07	-149	M	11/04 07:54	523	360	C5.2	AR8375	N17E01	SH+ICME+**PICME-SH**	11/07 07:36(A)	11/07 22	11/09 03	2	F
			..	11/05 20:44	1119	360	M8.4	AR8375	N22W18	..	11/08 04:41(W)	..	..	..	
17	1998/11/09 18	-142	S	11/05 20:44	1119	360	M8.4	AR8375	N22W18	**MC**	11/08 04:41(W)	11/09 04	11/10 06	1	
18	1998/11/13 22	-131	S	11/09 18:17	325	190	NO	QS	N18E00	**MC**	11/13 01:43 (SC)	11/13 04	11/14 12	1	F
19	1999/01/14 00	-112	S	DG	..	..	NO	DG	DG	SH+**ICME**	01/13 10:47(W)	01/13 15	01/13 23	3	F
20	1999/02/18 10	-124	S	02/16 02:49(F)	..	..	M3.2	AR8458	S23W14	**SH**+ MC	02/18 02:48(W)	02/18 10	02/19 11	2	F
21	1999/09/23 00	-173	S	09/20 06:06	604	360	C2.8	QS	S21W05	**ICME**	09/22 12:09(W)	09/22 19	09/24 02	1	
22	1999/10/22 07	-237	S	10/18 00:06	144	240	No	QS	S26E08	**ICME - CIR**	10/21 02:20(W)	10/21 08	10/22 07	1	
23	1999/11/13 23	-106	M	DG	..	..	..	DG	DG	ICME+**PICME-SH**	11/13 12:48(W)	11/12 10	11/13 18	3	F
24	2000/02/12 12	-133	S	02/10 02:30	944	360	C7.3	AR8858	N22E03	SH+**ICME**	02/11 23:34(W)	02/12 09	02/13 00	1	
25	2000/04/07 01	-288	S	04/04 16:32	1188	360	C9.7	AR8933	N16W66	**SH**+ICME	04/06 16:32(W)	04/07 04	04/08 06	1	
26	2000/05/24 09	-147	M	05/20 06:26	557	..	C7.6	AR8998	S15W08	**ICME- ICME**	05/22 17	05/23 09	05/23 21	2	F
			..	05/22 01:50	649	360	C6.3	AR9004	N20W22	..	05/23 23:42(W)	05/24 12	05/26 18	..	
27	2000/07/16 01	-301	S	07/14 10:54	1674	360	X5.7	AR9077	N22W07	SH+**MC**	07/15 14:15(W)	07/15 19	07/17 08	1	
28	2000/08/11 07	-106	S	08/06 23:06	281	133	NO	UNK	UNK	SH+**MC**	..	08/10 19	08/12 01	3	F
29	2000/08/12 10	-235	S	08/09 16:30	702	360	C2.3	AR9114	N11W11	SH+**MC**	08/11 18:49(W)	08/12 05	08/13 22	1	
30	2000/09/18 00	-201	M	09/16 05:18	1215	360	M5.9	AR9165	N14W07	**SH(M)**+ICME(M)	09/17 15	09/17 21	09/21 12	2	
			..	09/15 21:50	285	360	C7.4	AR9165	N12E04	..	..	..	..	..	
			..	09/15 15:26	481	217	M2.0	AR9165	N12E07	..	..	..	..	..	
			..	09/15 12:06	633	235	C9.5	AR9165	N13E08	..	..	..	..	..	
31	2000/10/05 14	-182	M	09/29 21:50	173	274	NO	UNK	UNK	MC+PMC-SH+**ICME**	10/03 01:02(W)	10/03 10	10/05 06	2	F
			..	10/01 17:50	586	136	C5.0	QS	S27E33	..	10/05 03:28(W)	10/05 13	10/07 11	..	
32	2000/10/14 15	-107	S	10/09 23:50	798	360	C6.7	AR9182	N01W14	SH+**MC**	10/12 22:33(W)	10/13 12	10/14 20	1	
33	2000/10/29 04	-127	S	10/25 08:26	770	360	C4.0	QS	N06W60	SH+**MC**	10/28 09:30(W)	10/28 21	10/29 22	1	F
34	2000/11/06 22	-159	S	11/03 18:26	291	360	NO	UNK	UNK	**SH**+MC	11/06 09:30 (W)	11/06 22	11/07 17	3	F
35	2000/11/29 14	-119	M	11/26 17:06	980	360	X4.0	AR9236	N18W38	**ICME(M)**	11/28 05:25 (W)	11/28 16	11/29 22	2	F
			..	11/25 19:31	671	360	X1.9	AR9236	N20W23	..	..	..	..	..	
36	2001/03/20 14	-149	S	03/16 03:50	271	281	NO	UNK	UNK	SH+**MC**	03/19 11:33(W)	03/19 17	03/22 06	3	F

continued on next page

Solar and Interplanetary Sources of the 78 Major Geomagnetic Storms during 1996–2004

1	2	3	4	5	6	7	8	9	10	11	12	13	14	15	16
ID[a]	Dst (min)		S-IP[b]	CME			Flare	Source[d]	Source[e]	IP Solar Wind[f]	Shock[g]	ICME		CL[h]	FN[i]
	Time (UT)	Int. (nT)	Driver (Type)	Time[c] (UT)	Vel km/s	AW (d)	Class	Region (Type)	Coord.	Structure (Type)	Time (UT)	Start (UT)	End UT		
37	2001/03/31 09	-387	M	03/29 10:26	942	360	X1.7	AR9393	N20W19	SH(M)+ICME(M)	03/31 01:14(W)	03/31 05	04/03 15	2	
			..	03/28 12:50	519	360	M4.3	AR9393	N16E03	..	..	..	..	..	
38	2001/04/12 00	-271	M	04/10 05:30	2411	360	X2.3	AR9415	S23W09	SH(M)+MC(M)	..	04/11 22	04/13 07	2	
			..	04/09 15:54	1192	360	M7.9	AR9415	S21W04	..	..	..	..	..	
39	2001/04/18 07	-114	S	04/15 14:06	1199	167	X14.4	AR9415	S20W85	SH+MC	04/18 00:49(W)	04/18 12	04/20 11	1	F
40	2001/04/22 16	-102	S	UNK	..	..	NO	UNK	UNK	MC	04/21 15:29(W)	04/21 23	04/23 08	3	F
41	2001/08/17 22	-105	S	08/14 16:01	618	360	C2.3	AR9577	N16W36	SH+MC	08/17 11:01(W)	08/17 20	08/19 16	1	
42	2001/09/26 02	-102	S	09/24 10:30	2402	360	X2.6	AR9632	S16E23	SH+ICME	09/25 20:17(W)	..	..	1	
43	2001/10/01 09	-148	S	09/28 08:54	846	360	M3.3	AR9636	N08E19	SH+ICME	09/30 19:14(W)	10/01 08	10/02 00	1	
44	2001/10/03 15	-166	S	09/29 11:54	509	216	M1.8	AR9636	N13E03	MC	10/01 22	10/02 04	10/03 17	1	
45	2001/10/21 22	-187	S	10/19 16:50	901	360	X1.6	AR9661	N15W29	SH+ICME	10/21 16:40(W)	10/21 20	10/25 10	1	
46	2001/10/28 12	-157	M	10/25 15:26	1092	360	X1.3	AR9672	S18W19	PICME-SH	10/28 03:13(W)	..	..	2	
			..	10/24 06:26	597	145	C2.6	AR9675	S13E27	..	10/26 22	10/27 03	10/28 20?	..	
47	2001/11/06 07	-292	M	11/04 16:35	1810	360	X1.0	AR9684	N06W18	MC+PMC-SH+ICME	11/06 01:25(A)	11/06 13	11/09 06	2	F
			..	11/03 19:20	457	360	NO	DG	DG	..	11/05 10	11/05 19	11/06 06	..	
48	2001/11/24 17	-221	M	11/22 23:30	1437	360	M9.9	AR9704	S14W36	SH(M)+ICME	11/24 04:54(W)	11/24 14	11/26 00	2	
			..	11/22 20:30	1443	360	M3.8	AR9698	S25W67	..	11/24 05:51(W)	..	..	..	
49	2002/03/24 10	-100	M	03/19 11:54	860	180	M1.0	AR9866	S10W58	SH(M)+ICME(M)	03/23 11:24(W)	03/23 21	03/25 20	2	
			..	03/20 17:54	603	180	NO	AR9871	S21W15	..	..	..	..	..	
50	2002/04/18 08	-127	S	04/15 03:50	720	360	M1.2	AR9906	S15W01	SH+MC	04/17 11:01(W)	04/17 16	04/19 15	1	
51	2002/04/20 09	-149	S	04/17 08:26	1240	360	M2.6	AR9906	S14W34	SH+MC	04/19 08:25(W)	04/20 00	04/21 18	1	F
52	2002/05/11 20	-110	S	05/08 13:50	614	360	C4.2	AR9934	S12W07	SH+ICME	05/11 11:30	05/11 16	05/12 00	1	
53	2002/05/23 18	-109	M	05/22 00:06	1246	186	C9.7	AR9948	S25W64	SH(M)	05/23 10:44(W)	05/23 20	05/25 18	2	
			..	05/22 03:50	1557	360	C5.0	QS	S22W53	..	..	..	..	..	
54	2002/08/02 06	-102	M	07/29 12:07	562	154	NO	QS	N34W36	ICME+PICME-SH+MC	08/01 04:24(A)	08/01 09	08/02 00	3	F
			..	07/29 23:30	360	130	NO	UNK	UNK	..	08/01 23:09(W)	08/02 04	08/04 02	..	F
55	2002/08/21 07	-106	S	08/16 12:30	1585	360	M5.2	AR0069	S14E20	SH+MC	08/20 13	08/20 15	08/21 14	2	F
56	2002/09/04 06	-109	C	08/31 06:48(CH)	..	..	..	CH	S15	CIR	..	..	..	1	F
57	2002/09/08 01	-181	M	09/05 16:54	1748	360	C5.2	AR0102	N09E28	PICME-SH+ICME	09/07 16:22(W)	09/08 04	09/08 20	3	F
			..	..	..	..	..	..	..	..	..	09/07 10	09/08 04	..	
58	2002/10/01 17	-176	S	09/26 01:31	178	202	NO	UNK	UNK	SH+MC+CIR	09/30 07:54(W)	09/30 20	10/02 03	3	F
59	2002/10/04 09	-146	S	09/30 02:30	258	120	NO	QS	S17W17	SH+MC	10/02 22:41(W)	10/03 01	10/04 18	1	F
60	2002/10/07 08	-115	C	10/05 01:48(CH)	..	..	..	CH	S07	CIR	..	..	..	1	
61	2002/10/14 14	-100	C	10/11 02:39(CH)	..	..	..	CH	S26	CIR	..	..	..	1	
62	2002/11/21 11	-128	C	11/18 13:21(CH)	..	..	..	CH	S04	CIR	11/20 10:49(W)	..	..	1	F
63	2003/05/30 00	-144	M	05/28 00:50	1366	360	X3.6	AR0365	S11W12	SH(M)+ICME(M)	05/29 11:55(A)	05/29 13	05/29 18	2	F
			..	05/27 23:50	964	360	X1.3	AR0365	S0W17	..	05/29 18:31(W)	05/30 02	05/30 16	..	
			..	05/27 06:50	509	360	M1.6	AR0365	S07W14	..	..	..	..	..	
64	2003/06/18 10	-141	M	06/14 01:54	875	195	NO	QS	N22W15	SH(M)+ICME(M)+PICME-SH	06/16 18	06/17 07	06/18 09	2	F
			..	06/15 23:54	2053	360	X1.3	AR0386	S07E80	..	06/18 04:42(W)	..	..	..	
65	2003/07/12 06	-105	C	07/07 21:40(CH)	..	..	..	CH	N04	CIR	..	..	..	1	
66	2003/08/18 16	-148	S	0814 20:06	378	360	NO	UNK	UNK	SH+MC	08/17 13:45(A)	08/18 01	08/19 15	3	F
67	2003/10/30 01	-353	S	10/28 11:30	2459	360	X17.2	AR0486	S16E08	SH+MC	10/29 05:58(W)	10/29 11	10/30 03	1	F
68	2003/10/30 23	-383	S	10/29 20:54	2029	360	X10.0	AR0486	S15W02	SH+MC	10/30 16:19(W)	10/31 02	11/02 00?	1	
69	2003/11/20 21	-422	S	11/18 08:50	1660	360	M3.9	AR0501	N00E18	SH+MC	11/20 08:35(W)	11/20 10	11/21 01	1	F
70	2004/01/22 14	-149	S	01/20 00:06	965	360	C5.5	AR0540	S13W11	SH+ICME	01/22 01:05(A)	01/22 08	01/23 17	1	F
71	2004/02/11 18	-109	C	02/10 09:24(CH)	..	..	..	CH	N02	CIR	..	..	..	1	

continued on next page

Solar and Interplanetary Sources of the 78 Major Geomagnetic Storms during 1996–2004

1	2	3	4	5	6	7	8	9	10	11	12	13	14	15	16
ID[a]	Dst (min)		S-IP[b]	CME			Flare	Source[d]	Source[e]	IP Solar Wind[f]	Shock[g]	ICME		CL[h]	FN[i]
	Time (UT)	Int. (nT)	Driver (Type)	Time[c] (UT)	Vel km/s	AW (d)	Class	Region (Type)	Coord.	Structure (Type)	Time (UT)	Start (UT)	End UT		
72	2004/04/04 01	-112	S	03/31 10:36(F)	..	..	C3.4	AR0582	N16W10	**SH**+MC	04/03 09:00(A)	04/04 00	04/05 18	2	F
73	2004/07/23 03	-101	S	07/20 13:31	710	360	M8.6	AR0652	N10E35	SH+**ICME**	07/22 09:45(W)	07/22 18	07/24 08	1	F
74	2004/07/25 12	-148	S	07/22 08:30	899	132	C5.3	AR0652	N02E08	SH+**MC**	07/24 05:32(W)	07/24 14	07/25 15	1	F
75	2004/07/27 14	-197	S	07/25 14:54	1333	360	M1.1	AR0652	N04W30	SH+**MC**	07/26 22:25(W)	07/27 02	07/27 15	1	
76	2004/08/30 23	-126	S	08/25 13:31	108	182	NO	UNK	UNK	**MC**+CIR	08/29 09:09(W)	08/29 19	08/30 22	3	F
77	2004/11/08 07	-373	M	11/04 23:30	1055	293	M5.4	AR0696	N08E18	SH(M)+**MC(M)**	11/07 01:55(A)	11/07 22	11/09 10	2	
			..	11/04 09:54	653	360	C6.3	AR0696	S09E28	..	11/07 17:59(W)	..	..	..	
78	2004/11/10 10	-289	M	11/07 16:54	1759	360	X2.0	AR0696	N09W17	PICME-SH+**MC**	11/09 09:25(W)	11/09 20	11/23 20	2	F
			..	11/06 02:06	1111	214	M9.3	AR0696	N09E05	..	..	..	..	..	
79	2005/01/18 08	-121	M	01/15 23:06	2861	360	X2.6	AR0720	N16W05	**SH(M)**	01/17 07:15(A)	..	..	2	F
			..	01/15 06:30	2049	360	M8.6	AR0720	N16E04	..	..	..	..	..	
80	2005/01/22 06	-105	S	01/20 06:54	882	360	X7.1	AR0720	N12W58	SH + **ICME**	01/21 16:52(A)	01/21 20	01/22 17	1	
81	2005/05/08 14	-127	C	05/07 01:36(C)	..	..	..	CH	N10	**CIR**	..	..	..	1	
82	2005/05/15 08	-263	S	05/13 17:12	1128	360	M8.0	AR0759	N12E12	SH+**MC**	05/15 02:11(A)	05/15 06	05/17 12	1	
83	2005/05/20 09	-103	S	05/16 13:50	405	360	C1.2	AR0759	N13W29	**ICME**	..	05/20 04	05/21 05	1	F
84	2005/05/30 10	-138	S	05/26 15:06	586	360	B7.5	AR0767	S12E13	**ICME**	05/29 09:05(A)	05/31 01	05/30 23	2	F
85	2005/06/12 22	-106	S	06/09 14:35	377	125	C1.4	AR0776	N07E12	**MC**	06/12 04(A)	06/12 16	06/13 13	3	F
86	2005/08/24 11	-216	M	08/22 01:31	1194	360	M2.6	AR0798	S11W54	**SH(M)** + ICME(M)	08/24 05:45(A)	..	..	2	
			..	08/22 17:30	2378	360	M5.6	AR0798	S12W60	..	..	..	..	..	
87	2005/08/31 16	-131	C	08/29 10:48(C)	..	..	..	CH	S12	**CIR**	..	..	..	1	
88	2005/09/11 11	-147	S	09/09 19:48	2257	360	X6.2	AR0808	S10E58	SH+**ICME**	09/11 01:00(A)	09/11 05	09/12 07	2	F

[a] Event number in chronological order

[b] Solar and IP source type: S - single CME/ICME, M - multiple CMEs/ICMEs, C - Coronal Hole/CIR

[c] Time of first CME appearance in LASCO C2, except for (F), the onset time of the source flare, and (CH), the central meridian crossing time of the source coronal hole. "UNK" source unknown, "DG" LASCO data gap.

[d] Solar surface source region indicated by the NOAA active region number, or CH for a coronal hole, QS for a quiet Sun region, UNK if the source region can not be identified in the available observations, and DG for EIT data gap

[e] Surface source region heliographic coordinates. In the case of coronal holes, only the latitude is given. UNK and DG are defined as in footnote d

[f] Solar wind structures associated with the geomagnetic storm in time order. SH=sheath; ICME=interplanetary CME; MC=magnetic cloud. (M) indicates multiple structures of this type. "-" indicates an interaction between two structures, in particular, PICME-SH and PMC-SH denote a shock propagating through a preceding ICME or magnetic cloud respectively. Bold type indicates the structure associated with the peak of the storm; other structures that contribute to the storm (typically at the $>\sim -100$ nT level) are indicated in normal type.

[g] Shock passage time at ACE (A), WIND (W) or inferred from a geomagnetic storm sudden commencement (SC). If no shock is present, this is the arrival time of CME-driven disturbances.

[h] Overall confidence level of the solar source identification. "1" = unambiguous, with unanimous consensus from the Working Group members. "2" = more ambiguous, with several possible sources, but most group members agree on the identification listed. M-type events fall into this category because of their intrinsic complexity. "3" = ambiguous or problematic events. Events in this category are mostly driven by ICMEs with no obvious front-side halo CME counterpart identified. The CMEs listed are possible candidates; those without any surface signatures in the available observations are indicated by "UNK" in columns 9 and 10. See the footnotes and text for more discussion on the questionable events.

[i] Additional comments are in the footnote numbered according to the event number.

[2] Proposed CME 04/16 07 had no corresponding surface eruption signature in EIT. An alternative solar driver is an EIT dimming at 04/16 14 UT at S22E04. However, this dimming has no corresponding CME in LASCO.

[4] Filament eruption, no EIT dimming. The surface source region is near NOAA AR8090.

[6] LASCO/EIT data gap, but C1 LDE flare, and cusp in SXT.

[7] Proposed CME 02/12 15 had no corresponding surface eruption signature in EIT. Partial halo CME 02/14 06 is too close to the ICME arrival time, because the slow solar wind and slow CME speed imply a longer transit time.

[9] A complex flow event involving multiple CMEs/ICMEs. The onset of this flow was caused by CME 04/29 17. The shock associated with the principle CME (05/02 14) driving the storm arrived at 05/04 02:15(A).

[10] Storm driven by the second MC. EIT data gap. Surface sources inferred from SXI.

[11] LASCO/EIT data gap. No major flare activity.

[12] LASCO/EIT data gap. No major flare activity.

[13] LASCO/EIT data gap. X1.0 LDE flare.

[14] LASCO/EIT data gap. M7.1 LDE flare

[15] Slow filament eruption.

[16] Bs mainly in the first ICME.

[18] The source region is in the quiet Sun between two active regions.

[19] LASCO/EIT data gap. No major flare activity.

[20] LASCO/EIT data gap. M3.2 flare

[23] LASCO/EIT data gap.

[26] Both CMEs are not in the original catalog. LASCO images indicated multiple CMEs interacting in the field of view.

[28] Surface source region of the 08/06 23 UT has not been identified. Maybe it is a backside CME? An alternative driver is the CME at 08/08 15 UT, but the source region is at N25W75, and this may be difficult to reconcile with a MC counterpart at the Earth.

[31] Three < -100 nT minima, caused by the magnetic cloud, a shock running into this magnetic cloud, and an ICME.

[33] Surface source region showed weak dimming in EIT and was between two active regions.

[34] Surface source region largely unknown. One possibility is a large-scale dimming spanning four small active regions (ARs 9218, 9213, 9212 and 9214) with a centroid at N10E05.

[35] Three FH CMEs on 11/24 may be also involved in the early part of the complex solar wind flow.

[36] CME 03/16 03 UT lacked a disc signature in EIT, so it may be a backside CME. An alternative source is the EIT eruption at 03/15 21 UT, but this did not produce a CME in LASCO.

[39] Big SEP, LASCO ""snowstorm"". However, the near-limb source may not be consistent with the MC present at 1 AU. An alternative source is the PH CME at 04/14 21 UT from N45E15.

[40] No good solar driver can be found. A filament eruption occurred at 04/17 13 UT close to southern polar region, but it produced a narrow and weak CME not listed in the CME Catalog. PH CME at 04/19 12 UT from N19W22 corresponded to a transit time of about 50 hours, which was inconsistent with the slow ICME and CME speed.

[47] EIT data gap.

[51] Double *Dst* peak.

[54] GOES M4.7 flare at 07/29 10:27 UT was not associated with CME 07/29 12 UT.

[54] Surface source region for this CME can not be identified. There was no apparent eruption signature seen in EIT.

[55] PH CME 08/18 21 UT was too slow, not compatible with a 1000 km/s transit speed. But CME 08/16 12 must have slowed down significantly before reaching the Earth, possibly affected by a preceding CME.

[56] EIT data gap. CH central meridian transit time was extrapolated from earlier observations.

[57] M-type, what is the other solar CME? FH CME at 09/05 16 UT showed EIT dimming, wave and arcade.

[58] The CME was a gradual one, growing more promient in C3 than in C2. However, there was no apparent eruption signature seen in EIT. CIR was involved in the SW flow.

[59] CME not in the original CDAW catalog.

[62] EIT data gap. CH central meridian transit time was extrapolated from earlier observations.

[63] SMEI halo CME (best one); 5/28, 16:53 thru 5/29. EIT 304 instead of EIT 195 observations.

[64] SMEI CME. EIT arcade associated with PH CME 06/14 01 UT.

[66] Strong halo CME, but no appreciable EIT signature: no dimming, no flare. There might be an extremely weak wave from S30E00.

[67] Two Dst dips.

[69] SMEI CME 11/19, 05:48. 50-75°.

[70] SMEI CMEs on 1/21, 03:49 and 22, 04:14. 35-80°.

[72] C3.4 LDE flare. Eruption seen in SXI. LASCO/EIT data gap. Halo CME in C3 at 04/01 00:25 UT. Sheath and cloud boundary unclear. SMEI CMEs 3/31 - 4/3. Out to 90°

[73] Complete chain is shown with SMEI. Shock and cloud boundary unclear.

[74] SMEI CME loops at 7/20, 21:29 and 21, 16:02 match LASCO CME structure well.

[76] CME 08/25 13 UT is gradual; apparent eruption signature seen in EIT. Could be a front-side CME? Or backside? An alternative driver is CME at 08/26 12 UT. However, the transit time was probably too short, not compatible with the CME and ICME speeds.

[78] SMEI CME 11/8, 19:22: several parts or events. 40-85°.
[79] No clear ejecta signatures.
[83] No CME-driven shock.
[84] EIT 304 only.
[85] EIT data gap. Source CME inconclusive.
[88] LASCO/EIT data gap from 09/07 to 09/09.

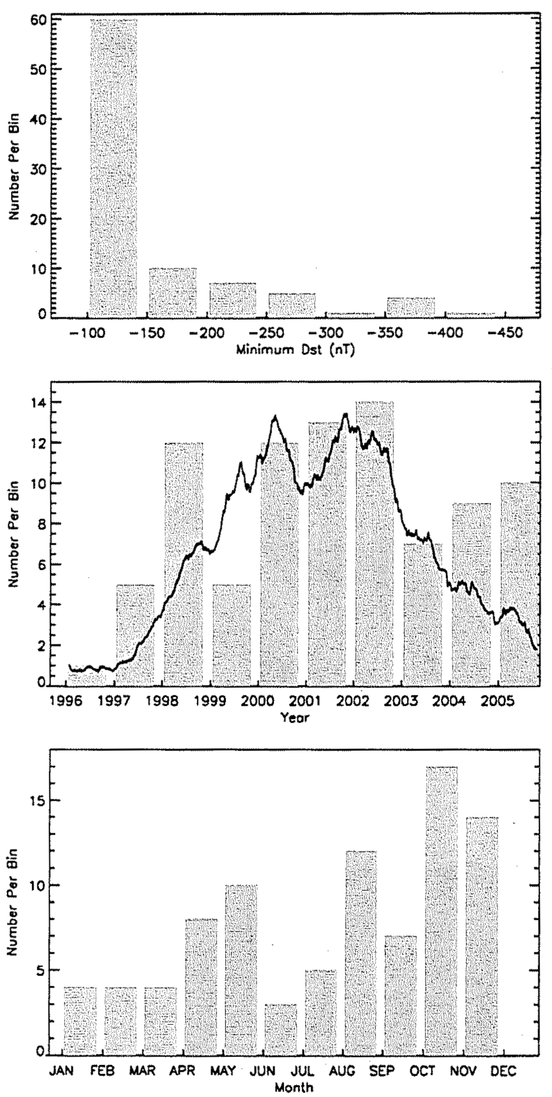

Figure 1. Distributions of the minimum Dst (upper panel, bin size = 50 nT), yearly occurrence rate (middle panel), and occurrence rate per calender month (lower panel) for 88 major geomagnetic storms during 1996 – 2005. The black curve overlaid in the middle panel shows the 180-day-running-average daily sunspot numbers in arbitrary units

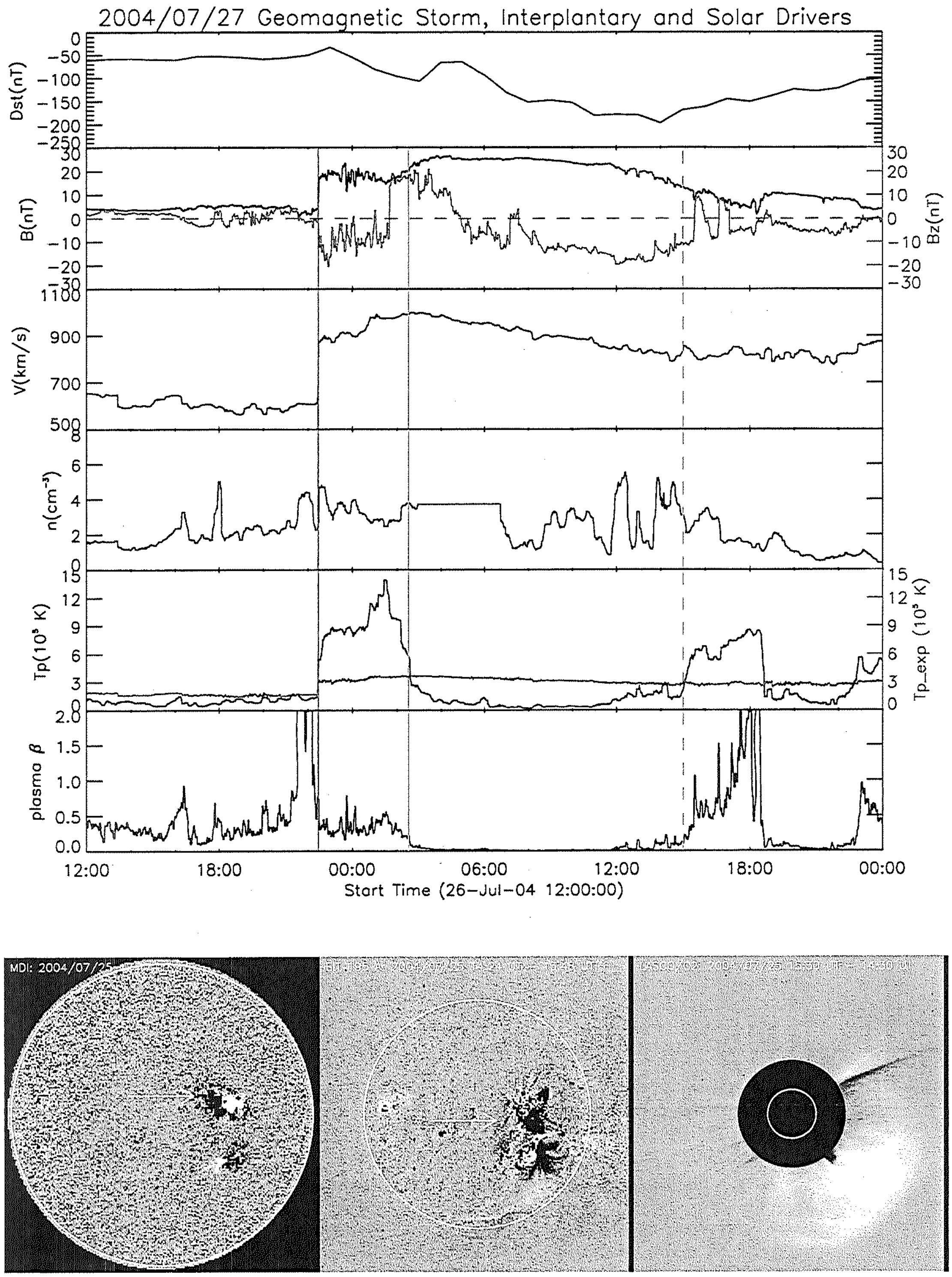

Figure 2. Geomagnetic, interplanetary and solar data related to the major geomagnetic storm (minimum $Dst = -197$ nT) on July 27, 2004 (event 75). The upper six panels, from top to bottom, show temporal profiles of the Dst index, solar wind magnetic field intensity (black) with the B_z component (red) overlaid, solar wind velocity, density, and proton temperature (black) overlaid with the expected temperature (red) (Richardson and Cane, 1995), and the plasma β. The solar wind data are from ACE in GSE coordinates. The solid and dotted blue vertical lines indicate the starting and ending times of the ICME, which in this case is a magnetic cloud. The vertical red line indicates the arrival time of the ICME-driven shock. The three images at the bottom, from left to right, indicate the source active region in a SOHO/MDI magnetogram for July 25, the coronal brightening accompanying the associated CME observed by EIT (running difference image), and this CME shown in a LASCO C2 coronagraph running difference image.

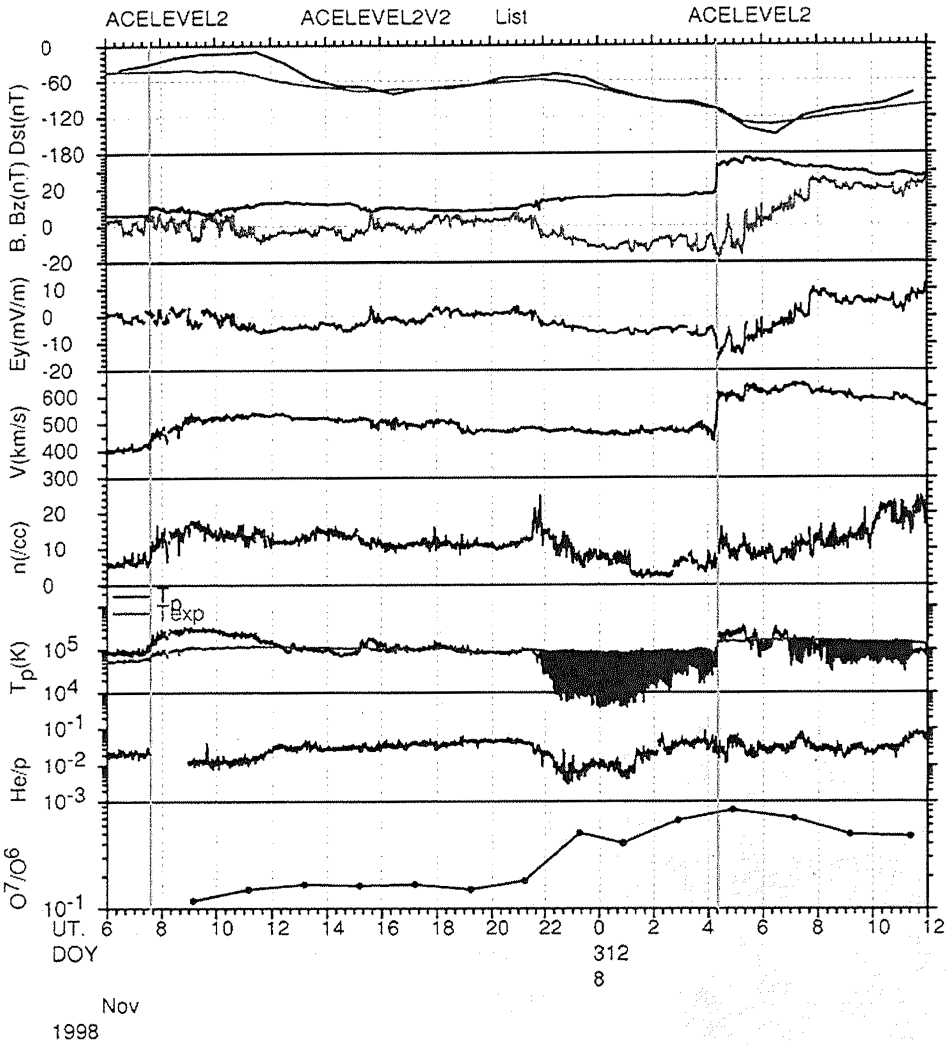

Figure 3. Geomagnetic and interplanetary data for the major geomagnetic storm (minimum $Dst = -149$ nT) on November 8, 1998 (event 16). The panels show, from top to bottom, the observed Dst (black) with the predicted Dst index using the O'Brien & McPherron formula [2000] overlaid in red, the magnetic field intensity (black) with B_z overlaid in red, the Y-component of the solar wind electric field, the solar wind velocity, density, proton temperature (black) and expected proton temperature (red) with the shaded black shading indicating where the proton temperature falls below the expected temperature, Helium/proton ratio, and O^7/O^6 ratio. The two vertical green lines indicate the arrival times of ICME-driven shocks. Here, the peak of the storm is caused by an interplanetary shock ($\sim$ 04 UT on November 8) propagating through a preceding ICME which has an embedded strong southward magnetic field.

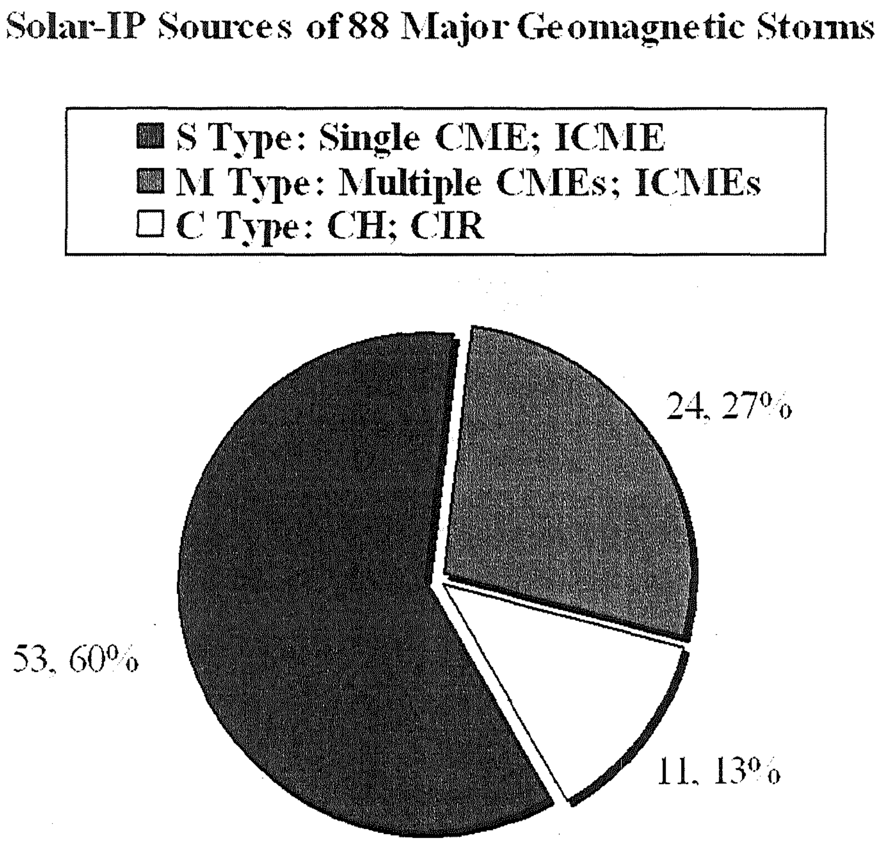

Figure 4. Distribution of the three types of solar-IP sources for the 88 major geomagnetic storms during in 1996 – 2005.

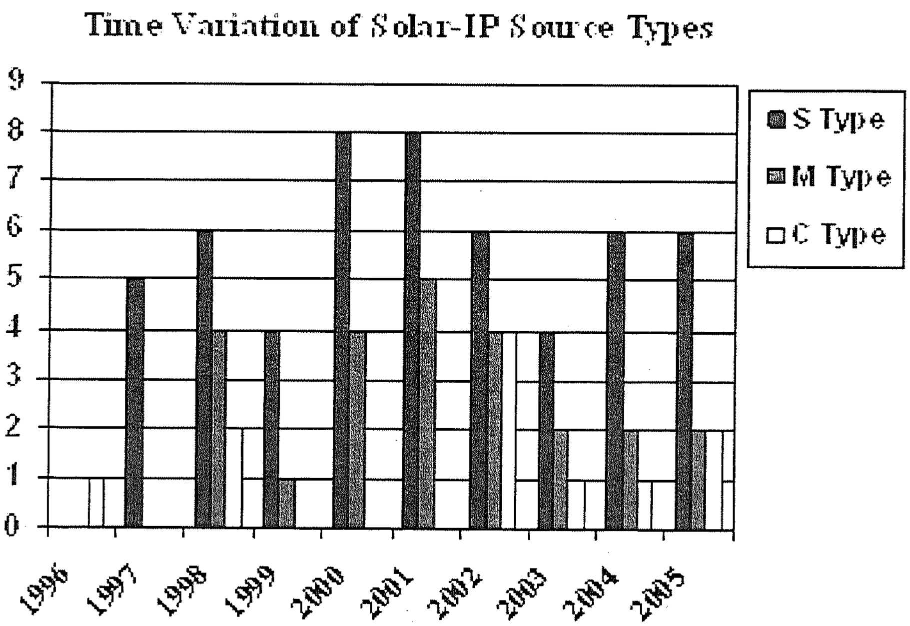

Figure 5. Solar cycle variation of the occurrence rate of the three types of solar-IP sources for the 88 major geomagnetic storms during 1996 – 2005.

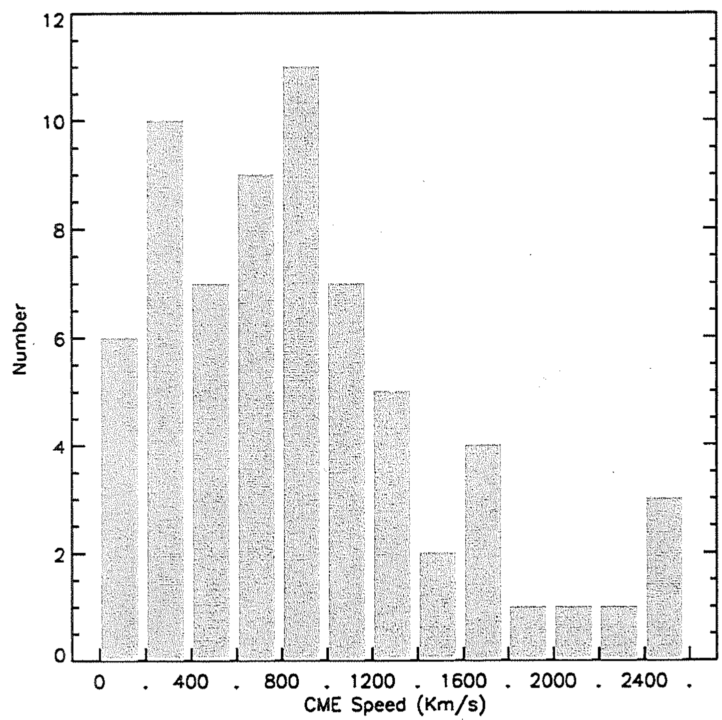

Figure 6. Distribution of the plane of the sky speeds for the 68 CMEs observed by SOHO/LASCO that resulted in major storms.

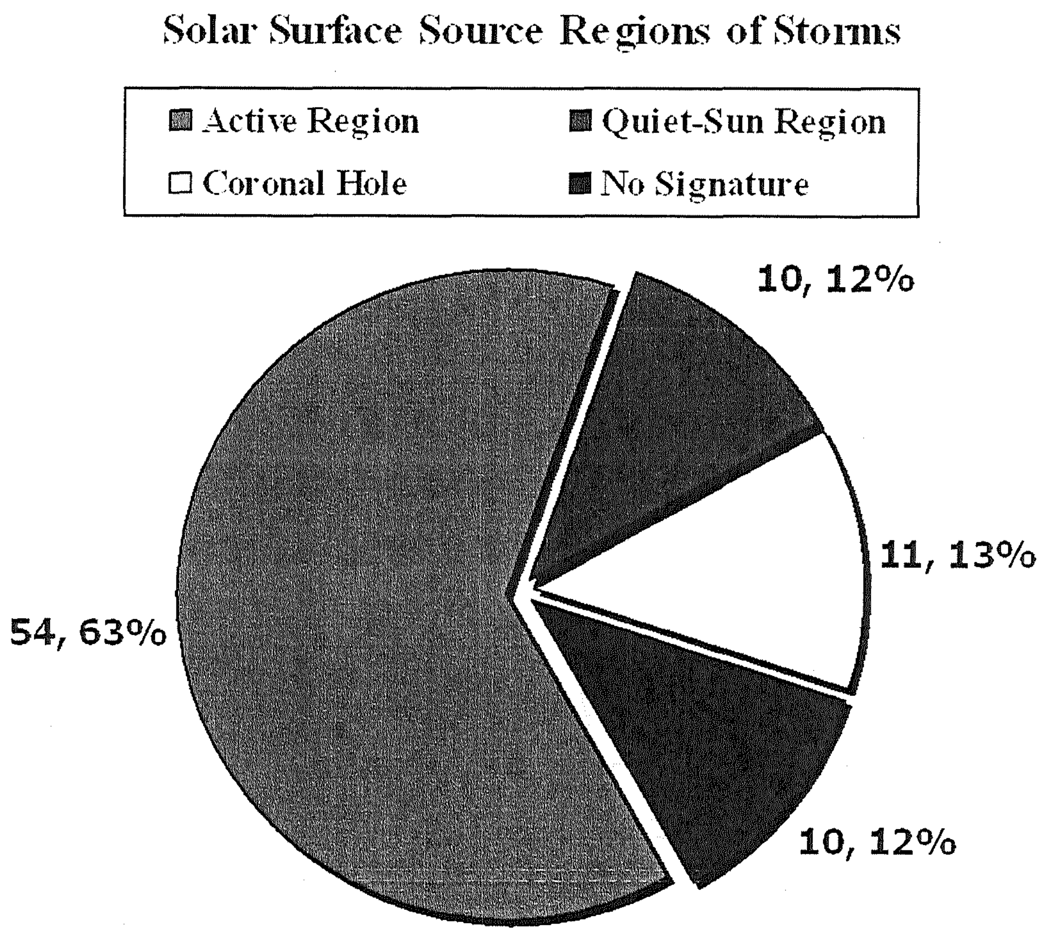

Figure 7. Types of solar surface source regions for the 88 major geomagnetic storms during 1996 – 2005.

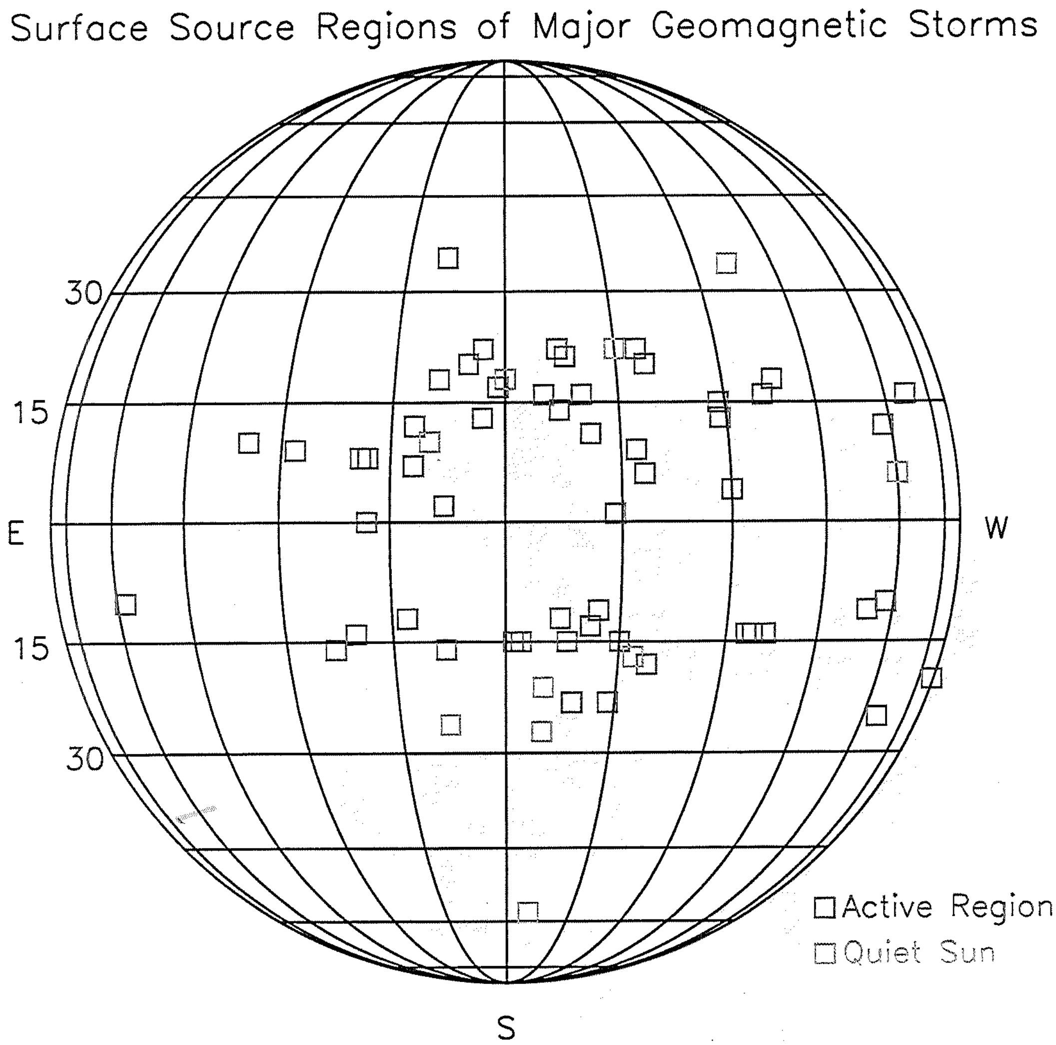

Figure 8. Heliographic locations of the 64 identified surface source regions for the CMEs that resulted in major geomagnetic storms during 1996 – 2005.